Received: 25 June 2023 | Revised: 26 September 2023 | Accepted: 10 November 2023

DOI: 10.1002/mp.16842

AAPM SCIENTIFIC REPORT

MEDICAL PHYSICS

Joint AAPM Task Group 282/EFOMP Working Group Report: Breast dosimetry for standard and contrast-enhanced mammography and breast tomosynthesis

Ioannis Sechopoulos[1,2,3] | **David R. Dance**[4] | **John M. Boone**[5] | **Hilde T. Bosmans**[6] | **Marco Caballo**[1] | **Oliver Diaz**[7] | **Ruben van Engen**[2] | **Christian Fedon**[8] | **Stephen J. Glick**[9] | **Andrew M. Hernandez**[5] | **Melissa L. Hill**[10] | **Katie W. Hulme**[11] | **Renata Longo**[12] | **Carolina Rabin**[13] | **Wendelien B. G. Sanderink**[1] | **J. Anthony Seibert**[5]

[1]Radboud University Medical Center, Nijmegen, The Netherlands

[2]Dutch Expert Centre for Screening (LRCB), Nijmegen, The Netherlands

[3]University of Twente, Enschede, The Netherlands

[4]National Co-ordinating Centre for the Physics of Mammography (NCCPM), Royal Surrey County Hospital, Guildford, UK

[5]University of California, Davis, California, USA

[6]KU Leuven, Leuven, Belgium

[7]University of Barcelona, Barcelona, Spain

[8]Radboud University Medical Center (now at Nuclear Research and Consultancy Group, NRG), Nijmegen, The Netherlands

[9]Food and Drug Administration, Silver Spring, USA

[10]Volpara Health, Wellington, New Zealand

[11]Cleveland Clinic, Beachwood, USA

[12]University of Trieste, Trieste, Italy

[13]University of the Republic, Montevideo, Uruguay

Correspondence
Ioannis Sechopoulos, Department of Medical Imaging, Radboud University Medical Center, P.O. Box 9101 (766), 6500 HB Nijmegen, The Netherlands.
Email: ioannis.sechopoulos@radboudumc.nl

Abstract

Currently, there are multiple breast dosimetry estimation methods for mammography and its variants in use throughout the world. This fact alone introduces uncertainty, since it is often impossible to distinguish which model is internally used by a specific imaging system. In addition, all current models are hampered by various limitations, in terms of overly simplified models of the breast and its composition, as well as simplistic models of the imaging system. Many of these simplifications were necessary, for the most part, due to the need to limit the computational cost of obtaining the required dose conversion coefficients decades ago, when these models were first implemented.

With the advancements in computational power, and to address most of the known limitations of previous breast dosimetry methods, a new breast

dosimetry method, based on new breast models, has been developed, implemented, and tested. This model, developed jointly by the American Association of Physicists in Medicine and the European Federation for Organizations of Medical Physics, is applicable to standard mammography, digital breast tomosynthesis, and their contrast-enhanced variants. In addition, it includes models of the breast in both the cranio-caudal and the medio-lateral oblique views. Special emphasis was placed on the breast and system models used being based on evidence, either by analysis of large sets of patient data or by performing measurements on imaging devices from a range of manufacturers. Due to the vast number of dose conversion coefficients resulting from the developed model, and the relative complexity of the calculations needed to apply it, a software program has been made available for download or online use, free of charge, to apply the developed breast dosimetry method. The program is available for download or it can be used directly online. A separate User's Guide is provided with the software.

KEYWORDS
dosimetry, mammography, tomosynthesis

1 | INTRODUCTION

1.1 | Charge

The American Association of Physicists in Medicine (AAPM) and the European Federation of Organizations for Medical Physics (EFOMP) established the joint AAPM Task Group (TG) 282/EFOMP Working Group (WG) in April 2016 with the aim to develop and disseminate an improved model and corresponding methodology to estimate the breast average glandular dose (D_g) from x-ray based image acquisitions, including standard mammography, contrast-enhanced mammography, and digital breast tomosynthesis.

1.2 | Background

Being widely used for screening for breast cancer, mammography and digital breast tomosynthesis are among the most commonly used radiographic tests in the world. Therefore, although these imaging modalities result in low dose to the imaged breast, their widespread use in asymptomatic individuals calls for a comprehensive understanding of their dosimetry. A model that allows for an appropriate estimation of the radiation dose to the breast, and its variation with image acquisition parameters and breast characteristics, is needed to, most importantly, optimize imaging systems and their acquisition protocols, perform various quality control procedures (such as type, acceptance, and periodic testing), as well as to estimate any increase in risk for development of breast cancer.

However, D_g due to mammography and its variants cannot be measured, only estimated, by measuring the quality and quantity of the radiation incident on the breast and using computer-obtained factors to convert this measurement to D_g. Therefore, models of the imaged breast and of the acquisition process need to be developed and used to obtain these conversion factors. Currently, various breast dosimetry models have been proposed in the literature and several of them are in use by the medical physics community, the imaging system vendors, and protocol-, standard-, and guideline-setting bodies. Dance and Sechopoulos have recently reviewed the history and current situation of breast dosimetry, and therefore the interested reader is referred to that work, and references therein.[1]

Briefly, most, if not all, current breast dosimetry methods involve the definition of standard breast(s), an x-ray field incident upon it, an air kerma (or exposure) measurement location, and a set of Monte Carlo simulation-derived air kerma-to-absorbed dose conversion factors. In general, the standard breasts are simple half-cylinders, reflecting the breast while compressed for acquisition of a cranio-caudal (CC) view image. The breast is defined as being composed of an outer layer of skin or adipose tissue, with an interior tissue composition of a homogeneous mixture of adipose and fibroglandular tissue, with varying relative concentration of each. Usually, the x-ray field does not include the variation in air kerma incident upon the breast due to the heel effect. In most cases, the conversion factors have been derived and/or published for x-ray spectra as produced by the different targets and added filters common in breast imaging.

As described by Dance and Sechopoulos, current models have various limitations.[1] In the first place, the mere existence of various models results in confusion among the community. It is in many cases not clear which model and methodology an imaging system is using internally, making it difficult to compare

manually obtained dose estimates to those displayed by the system. Sometimes, the same imaging systems installed in different countries are set internally to use different models, depending on the laws, guidelines, or preferences in that country. In some cases, the model used by the system is specified in the accompanying documentation, but this is not always the case, and it is not easily apparent to the user. In addition, some implementations include simplifications of the model used.

As mentioned, most current models only attempt to reflect D_g during acquisition of the CC view, although the medio-lateral oblique (MLO) view is also acquired during screening. Due to the difference in overall shape of the breast and location in the x-ray field, and especially due to the inclusion of a portion of the pectoralis muscle in the field of view, the conversion factors for the MLO-view breast are expected to be different than those for the CC view.[2]

Due to the development and publication of conversion factors corresponding to specific x-ray spectra, the introduction of new materials for the additional filtration of the x-ray field, and the increase over time in the tube voltages used in digital mammography, has previously necessitated the continuous computation and publication of new conversion factors. The introduction of contrast-enhanced spectral mammography to the clinical realm has increased this need, with the addition of even more filters and an expansion of the tube voltage ranges needed to be considered. This results in the need for repeated updating and publishing of tables of conversion coefficients.[3–10]

Most importantly, the recent introduction of dedicated breast computed tomography has allowed for a novel comprehension of breast composition and anatomy and its impact on breast dosimetry estimates. In the first place, new information is now available on the thickness of the skin,[11] and the distribution of the fibroglandular tissue throughout the breast.[12] In addition, the actual range of breast densities in the screening population, the portion of internal breast tissue that consists of fibroglandular tissue instead of adipose tissue, is now better understood.[13] Previous assumptions that the average breast density was 50%[14] have now been replaced with a more accepted model of the average density being closer to 15%.[13]

This new characterization of breast anatomy has shown that current breast models tend to over-estimate D_g during mammography in the vast majority of cases. In fact, on average this over-estimation has been estimated to be about 30%.[15,16] Although the aim of these dose models is not to reflect the dose to any individual breast due to any specific acquisition, it is desirable that the model dose is an accurate estimate of the dose to an average patient breast of the same thickness.

1.3 | Aim

Therefore, based on the above and other factors identified in the current breast dosimetry models, the aim of this joint TG/WG was to develop a breast dosimetry model with the following characteristics:

- Applicable to mammography and digital breast tomosynthesis, and their contrast-enhanced variants.
- Compressed breast shapes reflecting both CC and MLO views.
- Inclusion of the pectoralis muscle in the MLO view.
- Breast model representative of current understanding of breast anatomy, including:
  - Different breast sizes for different compressed breast thicknesses.
  - Appropriate breast skin thickness definition.
  - Fibroglandular tissue magnitude and distribution reflective of that found in the population.
- Realistic x-ray fields including the heel effect and major components of the x-ray systems.
- Computation of mono-energetic conversion factors, allowing for the computation of spectral conversion factors for any x-ray spectrum without the need for follow-up publications.
- Definition of a single new reference incident air kerma and a simplified method to determine it.
- Release of easily accessible computer software to obtain the average glandular dose estimates from measurements of air kerma.

It is the aim of this joint TG/WG that the model and methodology described herein replaces all currently used breast dosimetry models, thereby achieving hegemony and uniformity in the breast dosimetry work performed by the medical physics community and our industry partners.

This Report describes the developed dosimetry model and the required inputs, the methodology for measuring the air kerma, the recommended values for the inputs to the model when these are unknown, and the characteristics and use of the developed software released together with this publication. In the next Section, the recommended nomenclature and symbols used throughout this Report are listed and defined. In Section III, an overview of the developed model and method are provided with an introduction to the included dosimetry software. Review of these two Sections should be sufficient to be able to use the developed breast dose model. Detailed instructions on the use of the dosimetry software are included in the User's Guide provided with the software. Further details on the entire methodology are provided in Section IV, including the basis for the dose conversion coefficients, the development of the breast and spectral models, the details of the Monte Carlo simulations, and the processing

performed by the dosimetry software. Finally, in the Appendices, additional information on various aspects of the model is provided and a comparison between D_g estimates obtained with this and previous models is made.

2 | NOMENCLATURE

2.1 | List of definitions and symbols

This joint TG/WG recommends and uses throughout this report the following terms and definitions:

- Average glandular dose (D_g): The absorbed dose to the fibroglandular tissue averaged over the entire imaged breast. D_g is expressed in units of milliGray (mGy).
- Measured air kerma (K_m): The air kerma, without backscatter, measured just above the breast support table, as described in Section III.B of this Report. K_m is expressed in units of milliGray (mGy).
- Reference air kerma (K_{ref}): The air kerma free-in-air, measured or estimated at the reference point. Reference air kerma is expressed in units of milliGray (mGy).
- Dose conversion coefficient (γ for monochromatic x rays, Γ for x-ray spectra): The coefficient to convert the reference air kerma to an estimate of the average glandular dose. Strictly speaking, the dose conversion coefficients are unitless, but can be expressed as having units of milliGray per milliGray air kerma (mGy/mGy).
- Source-to-K_m distance (l_m): The shortest distance between the x-ray source and the plane where K_m is measured. l_m is expressed in units of millimeters (mm).
- Source-to-support table distance (l_t): The shortest distance between the x-ray source and the breast support table. l_t is expressed in units of millimeters (mm).
- Reference point: The point on a plane 500 mm away from the x-ray source towards the imaging detector, centered laterally with the detector, and 40 mm in from the chest wall side edge of the x-ray field.
- Incident air kerma correction factor (c_k): Correction for differences beyond the inverse square distance relationship between K_m and K_{ref}.
- Volumetric breast density or breast density: The proportion of the total breast volume, including skin, occupied by fibroglandular tissue, in percentage (%), in whole numbers. In the case of the MLO view, both the numerator and denominator used to calculate this proportion exclude the portion of the breast (including skin, adipose/fibroglandular mixture, and pectoralis muscle) that is projected onto the pectoralis muscle at the imaging detector surface during imaging with the x-ray source positioned at the 0° position, equivalent to the DM/CEDM location.
- Phantom dosimetry or model dosimetry: Estimation of D_g using the K_{ref} resulting from using physical breast phantoms to drive the automatic exposure control (AEC) of an imaging system and breast model parameters as represented by those breast phantoms.
- Patient-based model dosimetry or patient-based dosimetry: Estimation of D_g using the K_{ref} resulting from the acquisition conditions obtained from records of actual breast acquisitions and the breast model parameters representative of typical breasts of that thickness.
- Prospective dosimetry: Equivalent to phantom dosimetry.
- Retrospective dosimetry: Equivalent to patient-based model dosimetry.
- Patient-specific dosimetry: Estimation of D_g using the K_{ref} resulting from the acquisition conditions obtained from records of actual breast acquisitions and the representation of the actual individual breast imaged in its true form. This includes the amount and location of the fibroglandular tissue in the breast. Note that patient-specific dosimetry is beyond the scope of this report, and it is impossible to perform in standard two-dimensional mammography.

2.2 | List of abbreviations

This joint TG/WG recommends and uses throughout this report the following abbreviations:

CC	Cranio-caudal
CEDBT	Contrast-enhanced digital breast tomosynthesis
CEDM	Contrast-enhanced digital mammography
DBT	Digital breast tomosynthesis
DM	Digital mammography
HVL	1st half-value layer
MLO	Medio-lateral oblique
PMMA	polymethyl methacrylate

3 | BREAST DOSIMETRY METHOD

3.1 | Breast dosimetry model

The fibroglandular tissue of the breast is the component most at risk for development of breast cancer. As such, breast dosimetry aims to estimate the absorbed dose to only this tissue of the breast. Given the currently accepted models of increased risk of development of cancer, which are whole-organ based,[17] and the strong gradients of absorbed dose in the breast due to the use of low energy x-rays,[18] the metric of interest in

breast dosimetry is the average of the absorbed dose to the fibroglandular tissue over the entire breast, denoted average glandular dose (D_g). Since D_g cannot be measured directly, it must be estimated, based on a reference air kerma and specific conversion factors, according to the following equation:

$$D_g = K_{ref}\,\Gamma \tag{1}$$

where D_g is the average glandular dose, in units of milliGray (mGy), K_{ref} is the reference air kerma free-in-air at 500 mm from the source and 40 mm anterior from the chest wall edge of the x-ray beam, in units of mGy, and Γ is the air kerma to dose conversion coefficient, which is, strictly speaking unitless, but can be thought of as having units of mGy/mGy.

The reference air kerma, K_{ref}, does not need to be measured at the defined location. Rather, a measurement of the air kerma, denoted K_m, can be taken at any distance, l_m, from the source, as long as the source, reference point, and measurement point are colinear, and from this measurement the K_{ref} can be calculated. For this dosimetry method, a specific location to measure K_m has been defined, as described in Section III.B.

However, due to the presence of the compression paddle in the x-ray beam, which introduces different amounts of forward scatter to K_m and K_{ref}, a correction factor, c_k, is needed for the correct conversion from K_m to K_{ref}. Since this correction factor was determined empirically, it includes any other small variations in forward- or back-scatter present at the measurement point compared to the reference point. The relationship between the two air kerma values is then given by:

$$K_{ref} = K_m\left(\frac{l_m}{500\ mm}\right)^2 c_k \tag{2}$$

Empirically, the value of c_k was established to be 1.032. Details on the method and results used to obtain this value are given in Appendix A. It should be noted that the 40 and 50 mm distances from the chest wall edge to the reference and measurement points (as described in Section III.B), respectively, introduce an additional geometric variation in the relationship between K_m and K_{ref} that is not taken into account in Equation 2. However, this variation, of the order of $< 0.1\%$ depending on the value of l_m, is inherently included in c_k.

As described in Section IV, the conversion coefficients Γ were obtained using Monte Carlo simulations for a specific image acquisition geometry and post-processed using a least squares fourth-order spline approximation method. In this simulated geometry, the distance from the source to the breast support table, and therefore to the bottom of the breast, was set to 648 mm. Therefore, these values need to be corrected for the actual distance from the source to the breast support table, l_t, of the system being assessed, using:

$$\Gamma = \Gamma_{sim}\left(\frac{648\ mm - t}{l_t - t}\right)^2 \tag{3}$$

where Γ_{sim} are the conversion coefficients obtained with the simulation geometry, and t is the compressed breast thickness, in mm. By using Equation 3, the coefficients are corrected to allow for the change in the incident air kerma at the top of the breast relative to that modelled in the Monte Carlo simulations.

In the case of contrast-enhanced applications, the acquisitions performed with the different x-ray spectra (low energy and high energy) should be treated as two separate acquisitions. Therefore, separate measurements of K_m should be performed and separate estimates of D_g should be obtained. The total dose for the CEDM or CEDBT exam is then the sum of the estimated D_g for the low energy (LE) and high energy (HE) acquisitions:

$$D_{g,CE} = K_{ref,LE}\,\Gamma_{LE} + K_{ref,HE}\Gamma_{HE} \tag{4}$$

The software included with this Report automatically performs the calculations described in Equations1, 2, and 3 for the acquisition technique and the breast characteristics specified. The details of how to measure K_m to be input into the program are described in Section III.B. The options available to describe the spectrum and breast to be used by the software program and to obtain the D_g estimate are provided in Section III.C. Finally, the use of the dosimetry software program is described in Section III.D and the step-by-step instructions for its use are given in the accompanying User's Guide.

3.2 | Measurement of air kerma

The measurement of air kerma should be performed only with the x-ray tube positioned at 0°, that is, at the DM/CEDM position. The setup to measure K_m is shown in Figure 1. As can be seen, the dosimeter should be placed on the breast support table, with the center of the active area of the dosimeter located on the centerline of the imaging detector perpendicular to the chest wall, and at the intersection of the breast support plane and a line extending from the source through the reference point. This point is approximately 50 mm in from the chest wall at the breast support table, and for practical purposes can be assumed to be at 50 mm. The compression paddle should be left in the beam but positioned as close to the x-ray tube output as allowed by the system. Finally, the collimation of the system to produce the largest x-ray field should be selected. It is recommended that

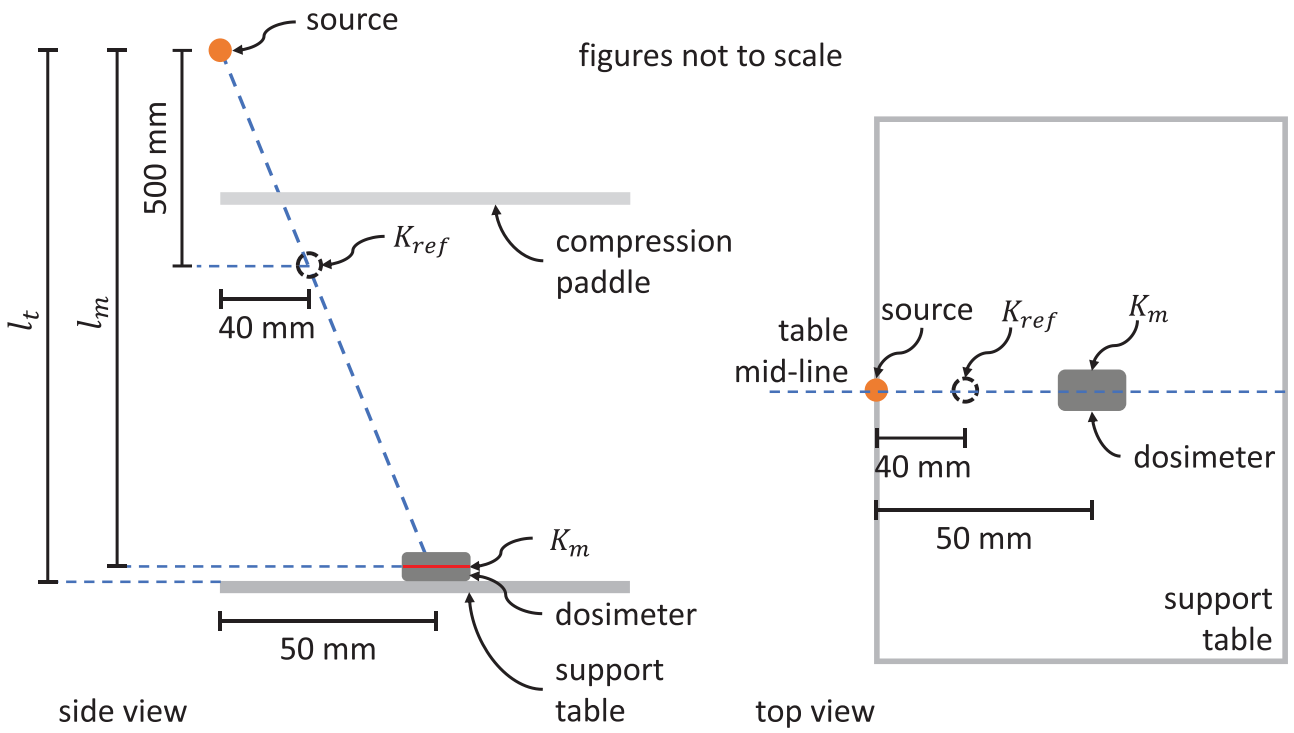

FIGURE 1 Schematic showing the setup for the measurement of the K_m and the location of the reference point at which K_{ref} is specified. The x-ray tube should be located at the DM/CEDM position. The red line on the dosimeter marks the effective measurement location of the dosimeter, and l_m is the vertical distance between this location and the source. l_t is the distance between the source and the top of the breast support table. The compression paddle should be placed between the source and the dosimeter, as close to the source as possible.

when performing these measurements some type of attenuating material (e.g., steel plate, lead apron, etc.) be placed on the breast support table, underneath the dosimeter, to protect the image receptor during repeated measurements.

Since the source to support-table distance varies across systems, in theory the distance between the chest wall edge and the projection of the air kerma reference point actually varies. However, for systems with source to support-table distances between 620 and 675 mm, this projected point varies only from 49.6 to 54.3 mm. As of the writing of this report, there are no systems that deviate substantially from this source-to-support table distance range. Therefore, this report recommends that the dosimeter should be placed on the breast support table with the center of the active area at 50 mm in from the chest wall edge for all systems. The error that this simplification may introduce across system geometries is minimal.

For dose estimations for magnification views, the air kerma should still be measured as suggested here, on the support table for the standard views. This ensures that the distance between the measurement location and the compression paddle is still as large as possible. The correct distance from the source to the magnification support table should then be entered for l_t.

The measurement can be performed with either an ionization chamber- or a solid-state detector-based dosimeter designed and calibrated for mammography. If performing CEDM/CEDBT, the calibration should be ensured to be also valid at the higher x-ray energies involved. As of this writing, it is known that solid-state dosimeters are backscatter insensitive, guaranteeing that the measurement performed with this setup is the air kerma **without backscatter**. Currently, this TG/WG understands that most, if not all, ionization chambers are also backscatter insensitive, but it is up to the medical physicist using this equipment to ensure that this is the case. If there is doubt as to whether the dosimeter used is backscatter insensitive, then this measurement can be performed with the dosimeter raised from the breast support table, at least 100 mm, so as to approximate a free-in-air measurement, keeping the measurement point colinear with the source and reference point. Along with K_m, the vertical distance between the source and the effective measurement location of the dosimeter (usually marked in the dosimeter), l_m, needs to be measured and recorded, since it is a required input to the dosimetry software, as shown in Equation 2, to determine the K_{ref} used by the dosimetry model.

The measurement of K_m should be made using a reasonable tube current-exposure time product, for example, 50 mAs, and then weighted by the actual tube

current-exposure time product for which D_g is being calculated. Note that for DBT acquisitions, the actual tube current-exposure time product value used should be that of the **total projection set acquisition**, not that of a single projection. As of this writing, the tube current-exposure time product input and displayed by all DBT systems is the total for the entire acquisition, and therefore no additional calculations need to be made. As specified later, the software allows for specifying non-constant tube current DBT protocols. In the case of contrast-enhanced calculations, the separate tube current-exposure time products corresponding to the LE and HE exposures should be used for each corresponding K_m measurement.

This setup for the measurement of the K_m was selected as it was deemed the most convenient and repeatable to perform. By placing the dosimeter directly on the breast support table, no special holder or separator is needed. Furthermore, the measurement no longer needs to represent the K_m at the entrance surface of the breast, which required a separate inverse-square-distance adjustment for each compressed breast thickness. In addition, allowing for the measurement to be performed with the full-field x-ray beam removes the need to use specific additional collimating shields of lead or other material.

As mentioned, the joint TG/WG evaluated the magnitude of the correction factor c_k needed to compensate for differences in x-ray scatter and any other errors introduced in the K_m measurements by the simplifications involved in this recommended setup, as opposed to measuring the actual K_{ref} free-in-air at the reference point. This is described in detail in Appendix A.

3.3 | Determination of average glandular dose

In addition to the measured incident air kerma, K_m, calculation of D_g requires modeling of the x-ray beam and the breast. The details for these two items are as follows.

3.3.1 | X-ray spectrum

Two different spectrum models can be used with the software to determine D_g: a system-specific model or a generic model. *The use of a system-specific model is strongly recommended and is the default option in the dosimetry software*.

System-specific spectrum model

For the dosimetry software to develop and use a spectrum model that is specific to the imaging system being evaluated, a measure of the 1st half value layer (HVL, in mm Al) for the x-ray spectrum being assessed is needed. This measurement should be performed with the breast compression paddle in the x-ray beam, again located as close to the x-ray tube output as possible. Instructions for how to measure the HVL are beyond the scope of this Report. In addition, the user must input the anode material (either molybdenum, rhodium, or tungsten), the tube voltage (between 20 and 49 kV), and the composition and thickness (in mm) of each added filtration used by the imaging system. In general, the composition and thickness of the added filtration is specified in the documentation of the imaging system. With these inputs, the x-ray spectrum is modeled by the software so that the model matches the measured HVL to within 1%. This is done by modifying the thickness of the additional filtration input with the highest atomic number until this maximum difference between measured and modeled HVL is achieved. It should be noted that manufacturer tolerances for the thickness of the additional filtration are usually ± 10%, therefore the adjustment performed here by the software to match the measured HVL is reasonable and expected, and is a common approach in spectrum modeling.

Generic spectrum model

If the HVL of the spectrum being analyzed is not known, then a generic model can be used. In this case, the software will use the spectrum as modeled given only the anode, tube voltage, and additional filtration inputs, and reports the HVL that the modeled spectrum gives.

3.3.2 | Breast model

The dose conversion coefficients were obtained from Monte Carlo simulations as described in Section IV. The dosimetry software uses two separate sets of coefficients, one for the compressed breast in the CC view, and another for the breast compressed for the MLO view. Therefore, the software user must select which view is desired. For other views, such as ML, LM, XCC, etc., this TG/WG recommends specifying the CC view as the model to be used by the software.

For both views, two different breast models can be used by the software: a population-based model or a generic model. *The use of the population-based model is strongly recommended and is the default option in the dosimetry software*.

Population-based breast model

The population-based model uses volumetric breast density data from a very large dataset of real breast DM images to set specific breast density percentages at each compressed breast thickness that are representative of the population of breasts encountered clinically (see Appendix B for details). To do this, the volumetric breast densities that correspond to the 5th, 25th, 50th (median), 75th, and 95th *percentiles* for a range of compressed breast thickness were obtained.

TABLE 1 List of *standard* breasts in the population-based breast model automatically evaluated by the dosimetry software program.

Breast thickness (mm)	20, 30, 40, 50, 60, 70, 80, 90
Volumetric breast density (percentile)	5^{th}, 25^{th}, 50^{th}, 75^{th}, 95^{th}

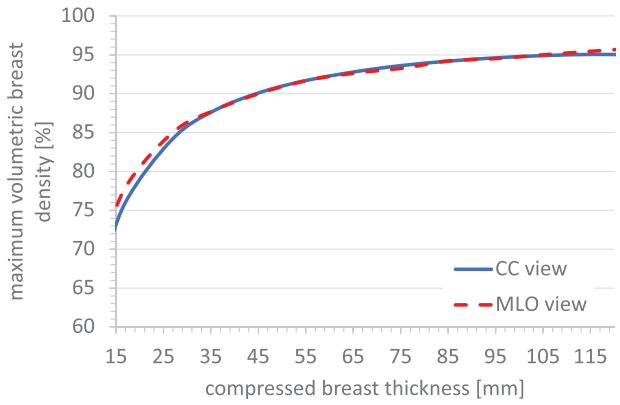

FIGURE 2 Dependence of the maximum volumetric breast density possible for the breast models for each view on compressed breast thickness.

The TG/WG recommends the use of percentile volumetric breast densities to define the composition of the breast models, so that the dosimetry estimates are performed for breasts with characteristics representative of those found in the population. The software can estimate the D_g for these five percentiles for a specified single compressed breast thickness, in the range 15 to 120 mm, or for the *standard* breast model set listed in Table 1. If the calculation of doses to this entire set of breast models in both views is desired, then the *standard* breast model set should be selected as the first input in the software accompanying this Report.

Generic breast model

The generic breast model allows for the specification of any single compressed breast thickness, ranging from 15 to 120 mm, and for any volumetric breast density, up to the equivalent of the internal breast tissue being composed of 100% fibroglandular tissue. If estimating D_g for a compressed breast thickness below 15 mm or above 120 mm is needed, then this TG/WG recommends that D_g to a 15 or a 120 mm thick compressed breast, respectively, be estimated. Furthermore, given the varied volume of the breast models occupied by the internal tissue, the skin, and the pectoralis muscle, the possible maximum volumetric breast density varies by view and breast thickness, as depicted in Figure 2. For any compressed breast thickness within the supported range, the software will calculate the maximum possible volumetric breast density for that thickness and accept input values of density up to this maximum. If this generic breast model is desired to be used, then no breast model set should be selected when prompted when using the accompanying software.

TABLE 2 List of EU legacy model breasts based on the use of PMMA slabs possible to be evaluated by the dosimetry software program.

PMMA thickness (mm)	Equivalent breast thickness (mm)	Equivalent volumetric breast density (%)
20	21	44
30	32	39
40	45	26
45	53	19
50	60	13
60	75	6
70	90	3

For legacy purposes, the software includes two specific *legacy* breast dose models to estimate the D_g for specific breast phantoms that, up to this writing, are commonly used. The EU legacy model defines the breasts to be evaluated as those closest to the set of standard breasts commonly used in Europe and other countries that are a result of the established equivalency between polymethyl methacrylate (PMMA) thicknesses and breasts thicknesses and densities, as listed in Table 2.[7] The US legacy model involves using a 42 mm thick breast model with 50% breast density by mass, representative of the American College of Radiology (ACR) accreditation phantom. Considering the description of that model by Wu et al.,[4] for the US legacy model the breast is defined as 42 mm thick with a 35% volumetric breast density.

Note that these resulting breast models are only approximately equivalent to the European standard breasts and to the ACR phantom since the shape of the breast models and the presence of the 1.5 mm skin layer does not allow for defining the exactly equal breasts.

3.4 | Dosimetry software

As previously mentioned, this report is accompanied by a software program that performs the calculations needed to estimate D_g for one or various breast exposures performed during acquisition of any of four different imaging modalities: DM, CEDM, DBT, and CEDBT. The software is made available, free of charge, for Windows, Mac, and Linux operating systems at https://doi.org/10.5281/zenodo.10030302. A web-based version of this program is also available for use at https://medphys.royalsurrey.nhs.uk/TG282doseCalculator. The underlying code of this software is available for system manufacturers to implement in their devices directly, upon request.

A separate User's Guide is provided together with the software that provides the most up-to-date information on the program inputs and outputs. Here an introduction to the software is provided, but any future changes that may be made to the software will be reflected on the separate user's guide. In case of any inconsistencies between this Report and the User's Guide of the software, the latter should be considered valid and up to date.

As of this writing, the program has four working modes, interactive, input-file based, batch processing, and graphical user input based. The functions performed by the program are the same in all modes, although when used with input files, a number of dosimetry calculations can be done with one execution. In addition, with input files, the projection angles in DBT/CEDBT can be irregularly spaced, and a variable tube current-exposure time product across projections can be specified. In interactive mode only a regular distribution of projection angles, symmetric about 0°, with constant tube output setting at each projection is allowed. Finally, in interactive mode, the number of dose estimations is limited to only a single breast or to the set of *standard breasts*, as listed in Table 1. Table 3 summarizes the inputs to the program, their format, and valid ranges.

As mentioned in Section III.B, the vertical distance from the source to the effective K_m measurement point (as marked on the dosimeter used), l_m, and to the breast support table, l_t, are needed. Both of these distances should be measured with the x-ray tube at the 0° position, equivalent to the DM/CEDM location (Figure 1).

It should be noted that for CEDBT acquisitions, the software program assumes that both the LE and HE acquisitions are performed at each and every projection angle listed. If this is not the case, two separate calculations need to be made.

For the contrast-enhanced modalities, a single breast and acquisition system specification is given, as for non-contrast DM and DBT, but two exposures are specified, one for the LE acquisition and one for the HE acquisition. This means that two sets of anode, tube voltage, additional filtration, and HVLs (if applicable) are to be provided.

4 | METHODOLOGY AND IMPLEMENTATION DETAILS

4.1 | Conversion coefficients Γ

In theory, the conversion coefficient Γ is obtained from the combination of multiple factors, including the mono-energetic version of these conversion coefficients, γ, according to the following equation:

$$\Gamma = \frac{\sum_{a=A_{min}}^{A_{max}} P(a) \sum_{e=E_{min}}^{E_{max}} \psi(e) \left(\frac{\mu_{tr}}{\rho}\right)_{air}(e)\, \gamma(t,\ g,\ e, a)}{P_{total} \sum_{e=E_{min}}^{E_{max}} \psi(e) \left(\frac{\mu_{tr}}{\rho}\right)_{air}(e)} \tag{5}$$

where:

$\sum_{a=A_{min}}^{A_{max}}$ is the sum over all projection angles included in the acquisition.

$\sum_{e=E_{min}}^{E_{max}}$ is the sum over all x-ray energies modeled to be included in the x-ray beam.

$P(a)$ is the tube current-exposure time product used for the acquisition at projection angle a.

P_{total} is the total tube current-exposure time product of the complete acquisition.

$\psi(e)$ is the modeled mono-energetic energy fluence of x-rays of energy e of the incident x-ray beam, at the reference point, when the x-ray source is positioned at the 0° projection angle.

$(\frac{\mu_{tr}}{\rho})_{air}(e)$ is the mass energy transfer coefficient in air for x-rays of energy e.

$\gamma(t,\ g,\ e, a)$ is the mono-energetic conversion coefficient from K_{ref} to D_g for the compressed breast of thickness t and density g, for x-rays of energy e at the a projection angle per unit air kerma at the reference point.

In short, the Γ spectral conversion coefficient is obtained from a set of mono-energetic $\gamma(t,\ g,\ e, a)$ coefficients that are a function of compressed breast thickness, breast fibroglandular density, x-ray energy, and projection angle. The interior sum in Equation 5 is to convert the mono-energetic coefficients to spectral coefficients. Therefore, the weighing factors are given by the relative contribution of the x-rays at each energy in the beam to the total air kerma, as specified by the spectrum model $\psi(e)$.

Because Equation 5 contains $\psi(e)$ in both the numerator and denominator, the energy fluence values in this model need not be normalized to any specific total energy fluence for the whole spectrum. In the case of DBT/CEDBT applications, as shown by the exterior sum in Equation 5, the projection-angle-specific spectral conversion coefficients are summed over all projection angles, to obtain the final Γ for the entire acquisition. The inclusion of the $P(a)$ in this sum and P_{total} in the denominator allows for any variation in the tube current-exposure time product with projection angle during DBT/CEDBT acquisitions.

To simplify the subsequent air kerma measurement needed to calculate D_g as per Equation 1, even for DBT and CEDBT exposures, the air kerma measurement is defined to be made only for the 0° projection, using the total tube current-exposure time product for the entire

TABLE 3 Summary of inputs to the dosimetry software program, with specification of the format required, units used, and valid ranges.

Input	Unit	Format	Valid range
Breast model			
Breast model set[a]	–	Text	Standard (default), EU, US, none
Breast view	–	Text	CC (default) or MLO
Breast thickness[b]	mm	Integer	15 – 120
Volumetric breast density percentile[b]	–	Integer	5, 25, 50 (default), 75, or 95
Volumetric breast density percentage[b,c]	%	Integer	1 – varies by thickness (see Figure 2)
Acquisition			
Modality	–	Text	DM (default), DBT, CEDM, or CEDBT
Source to dosimeter distance, l_m	mm	Integer	> 0
Source to breast support table distance, l_t	mm	Integer	> 0
DBT/CEDBT projection angle range	deg	Decimal	≥ 0.0 to ≤ 60.0
DBT/CEDBT number of projection angles[d]	–	Integer	≥ 1
DBT/CEDBT specific projection angles[d,e]	deg	Decimal	-30.0 – +30.0
DBT/CEDBT relative variation in tube current-exposure time product across projections[d,e]	–	Decimal	≥ 0.0
Spectrum model (in case of CE imaging, both low- and high-energy)			
Anode material	–	Text	Mo, Rh, or W
Tube voltage	kV	Integer	20 – 49
Filter elements[f]	–	Text	Any chemical element symbol
Filter thicknesses[f]	mm	Decimal	> 0.0
First half value layer	mm Al	Decimal	> 0.0
Measured air kerma, K_m	mGy	Decimal	> 0.0
Other program inputs			
Process pairs of breast thicknesses and densities[g]	–	Boolean	True/False
Adjust spectrum model to first HVL	–	Boolean	True/False

This information is accurate as of the publication of this Report. Any changes will be reflected in the accompanying User's Guide.
[a]If either the standard, EU, or US breast model set is input, then no other input for breast model is needed.
[b]Multiple values for these inputs can be specified in input-file mode.
[c]Only available when "none" is selected as breast model.
[d]If provided, the number of inputs for the exposure variation with projection angle must match the number of projection angles.
[e]Inputs available in input-file mode only.
[f]The number of inputs for filter element and thickness is unlimited, but they must be the same for these two inputs.
[g]If set to True, then an equal number of breast thicknesses and densities must be specified, and the program will process each pair of these inputs. If set to False, then all combinations of input thicknesses and densities will be processed.

DBT acquisition. Therefore, $\gamma(t,\ g,\ e, a)$ is actually normalized by the air kerma at the reference point when the x-ray source is at the 0° projection, regardless of the value of a.

Equation 5 is implemented in the dosimetry software program provided. Of course, in the case of DM and CEDM, Equation 5 can be reduced to the following, relevant only for mammographic acquisitions:

$$\Gamma = \frac{\sum_{e=E_{min}}^{E_{max}} \psi(e) \left(\frac{\mu_{tr}}{\rho}\right)_{air} (e)\, \gamma(t,\ g,\ e)}{\sum_{e=E_{min}}^{E_{max}} \psi(e) \left(\frac{\mu_{tr}}{\rho}\right)_{air} (e)} \quad (6)$$

Alternatively, if the DBT system uses a constant technique for all projection angles, as is the case for most current DBT systems, the exterior weighted sum in Equation 5 reduces to a simple summation with a division by the number of projections in the DBT acquisition:

$$\Gamma = \frac{\sum_{a=A_{min}}^{A_{max}} \sum_{e=E_{min}}^{E_{max}} \psi(e) \left(\frac{\mu_{tr}}{\rho}\right)_{air} (e)\, \gamma(t,\ g,\ e, a)}{N_a \sum_{e=E_{min}}^{E_{max}} \psi(e) \left(\frac{\mu_{tr}}{\rho}\right)_{air} (e)} \quad (7)$$

where:

N_a is the number of projections in the DBT/CEDBT acquisition.

TABLE 4 Characteristics of the breast phantoms developed for use in the Monte Carlo simulations to compute $\gamma_{sim}(t, g, e, a)$.

Parameter	Unit	Values
View	–	CC and MLO
Compressed thickness	mm	CC: 12, 17, 27, 36, 46, 56, 66, 75, 85, 95, 105, 115, 124
		MLO: 12, 17, 27, 36, 46, 56, 66, 76, 85, 95, 105, 115, 125
Fibroglandular density of the inner breast tissue, by mass	%	1, 10, 20, 30, …, 100

The resulting 286 breast phantoms are voxelized 3D arrays, with voxels of size 0.5 mm x 0.5 mm x 0.5 mm.[21] It should be noted that in this PCA-based breast model, the relationship between the PCA eigenvalue that mostly defines thickness and the resulting thickness of the breast is approximate, and that other eigenvalues have an effect on the relationship between shape and thickness. Therefore, the generated breast shapes are 1 or 2 mm from the desired input compressed breast thicknesses.

4.2 | Breast model

As discussed in Section I, the aim of this TG/WG in terms of the breast model was to develop separate models for the CC and MLO views that are representative of the exterior and interior characteristics of non-augmented breasts undergoing mammographic compression.

Although other mammographic views, such as spot views, magnification, medio-lateral, etc., are acquired clinically, especially for diagnostic purposes, the TG/WG decided to focus solely on the two standard CC and MLO views. This decision was based, to some extent, on the results of an investigation on the factors that affect the dose estimates in views involving partial irradiation, such as spot and magnification views.[19] Furthermore, other whole irradiation views, such as medio-lateral, caudal-cranial, etc., were excluded to limit the extent of the work to be performed. In any case, the CC and MLO views comprise the vast majority of mammographic acquisitions, especially after the introduction of DBT, which is replacing the use of other special diagnostic views.[20]

4.2.1 | Breast model representation and availability

The breast models were based on work performed to characterize the exterior shape and interior fibroglandular tissue distribution in actual compressed breasts. The overall process, resulting in the creation of 286 different voxelized breast phantoms, 143 for each view, with voxels of size 0.5 mm x 0.5 mm x 0.5 mm, is fully described by Caballo et al.[21] These 286 phantoms, used for the Monte Carlo simulations for determination of the dose conversion coefficients for the specific breasts simulated, $\gamma_{sim}(t, g, e, a)$, consist of breasts with the characteristics listed in Table 4.

Note that the fibroglandular density was specified in these phantoms by mass, and considering only the inner breast tissue (i.e., excluding the skin). However, most of the commercial and academic software that estimates breast density from DM and DBT images quantitatively, defines breast density differently. Specifically, breast density is quantified by volume, denoted *volumetric breast density*, and it is defined as the volume of the entire breast, including the skin, that is occupied by fibroglandular tissue. In addition, in the case of MLO-view images, these software algorithms first detect and exclude the area of the image containing the pectoralis muscle. Therefore, in the case of breasts compressed for this view, the volumetric breast density only considers the portion of the breast that does not project onto the same area of the image as the pectoralis muscle. Thus, to be consistent with clinical practice, the dosimetry software provided with this Report refers to and estimates dose to breast models defined by volumetric breast density as just described, not on density by mass. Therefore, the software performs the conversion required so that all breast densities are input and output by volume, including the breast skin in the calculation of the entire breast volume, and excluding the tissue that projects onto the same area as the pectoralis muscle in the MLO-view breast.

4.2.2 | Exterior breast shape

The exterior shapes of the breasts under compression are based on two previous publications, as follows.

4.2.3 | Two-dimensional shape

Rodriguez-Ruiz et al objectively analyzed the projected 2D shape of the compressed breasts in 1000 CC and MLO view mammograms using automated segmentation and principal component analysis (PCA).[22] In the case of the MLO view mammograms, the projection of the edge of the pectoral muscle was included in the analysis. From the results of the PCA, compressed breast thickness-dependent models, one for each view, were obtained. Using the models, the average shape and size of a breast of a user-specified compressed breast thickness can be generated. The external 2D shapes (including the edge of the pectoral muscle in the MLO view breasts) of 26 different breast models, 13 for each view, were thus generated corresponding to the thicknesses listed in Table 4.

It should be noted that, contrary to most previous breast dosimetry models, the breast area changes with compressed breast thickness, as shown in the examples in Figure 3.

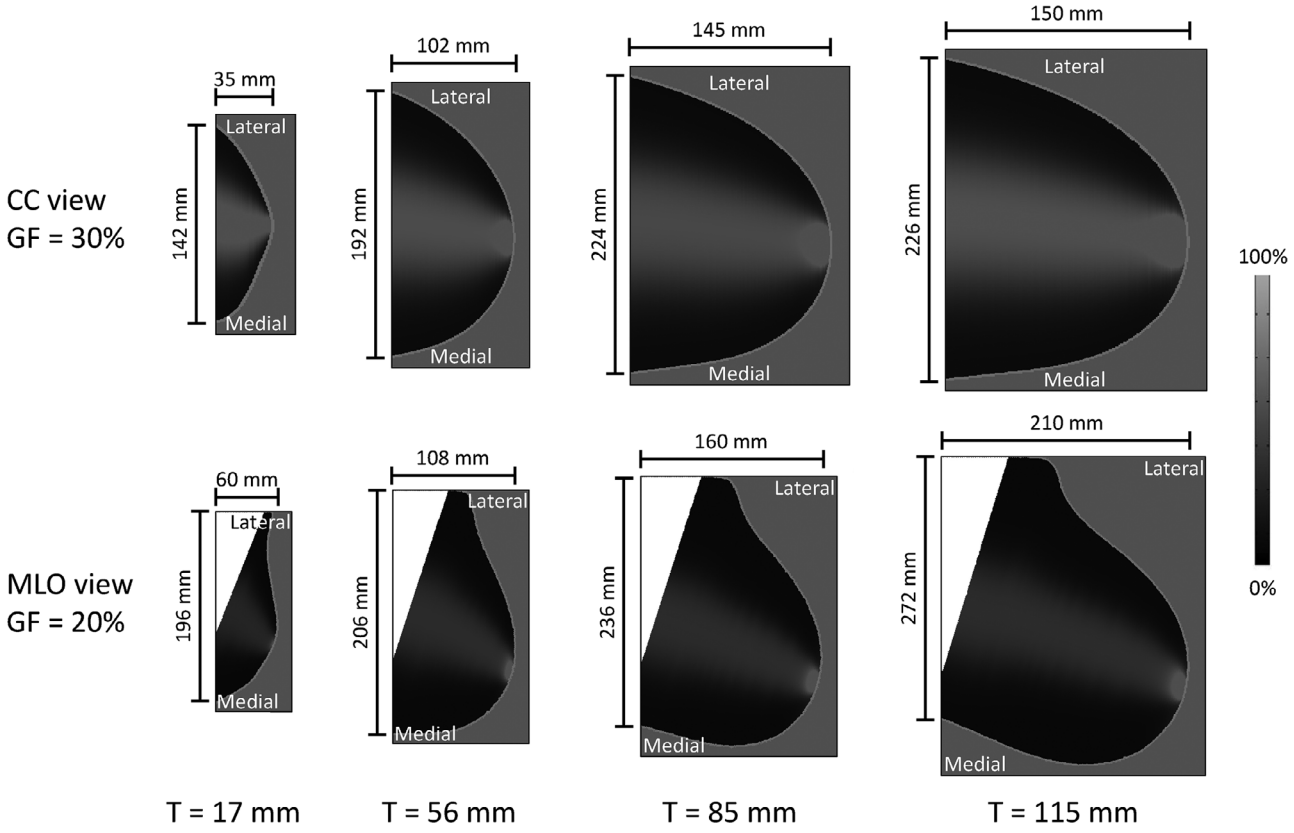

FIGURE 3 Examples of slices through the center of the breast models showing the variation in shape and size of the breasts with increasing compressed breast thickness. The internal grayscale variation shows the fibroglandular density distribution, by mass, throughout the depicted slice, while the white area in the MLO-view breast represents the pectoralis muscle. GF: glandular fraction; T: compressed breast thickness. Reprinted with permission from Caballo et al., Medical Physics, 2022;49(8): 5423–5438.

4.2.4 | Three-dimensional shape

To set the curvature of the breast models in the third dimension (i.e., between the breast compression paddle and the support table), the results of the characterization of this curvature in patient breasts undergoing compression by Rodriguez-Ruiz et al. were used.[23] In that work, the authors used a structured light surface scanning system to capture the vertical curvature of 45 breasts under compression for the CC view. From this information, another PCA-based model was obtained, which characterized the variation in this curvature with breast thickness. To do this, average-shaped model breasts were generated by setting the PCA eigenvalues to their corresponding population average values, except for the eigenvalue that mostly defines the breast thickness. This eigenvalue was set so to obtain the desired breast thickness for each breast model. From this model, the vertical profiles of compressed breasts of specific thicknesses for both views were generated (Figure 4), and combined with the 2D shapes generated above, to obtain the complete 3D shapes of the 26 breast phantoms corresponding to the first two rows in Table 4. It should be noted that the relationship between the PCA eigenvalue that mostly defines thickness and the resulting thickness of the breast, is approximate, and that other eigenvalues have an effect on the relationship between shape and thickness. However, to obtain average-shaped breasts, those other PCA eigenvalues need to be maintained at their population averages, so their slight impact on overall thickness cannot be compensated for. Therefore, the generated breast shapes are 1 or 2 mm from the input compressed breast thicknesses (e.g., the second thinnest breast was desired to be 15 mm thick, but the PCA-based method resulted in a 17 mm thick breast shape). Since all $\gamma_{sim}(t, g, e, a)$ values are the result of approximations across breast thicknesses, the accuracy of the dose estimates is not affected in any way.

4.2.5 | Interior breast tissue

The voxels located within the breast volume in the resulting shapes from the above process were defined to contain either skin or a homogeneous mixture of adipose and fibroglandular tissue of varying relative concentration of each, according to the following process. The chemical compositions and densities of the three tissues were set according to the work by Hammerstein et al.[14]

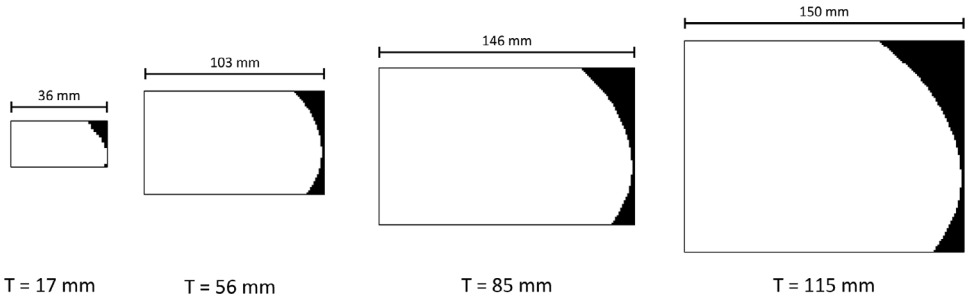

FIGURE 4 Examples of the breast model profiles showing the differences in curvature between the breast compression paddle and support table for breasts with increasing compressed breast thickness.

4.2.6 | Breast skin

Based on the work by Huang et al. on analysis of dedicated breast CT images of 100 breasts from 51 different women, the layer of skin for all breasts was set to 1.5 mm (i.e., three voxels thick).[11]

4.2.7 | Fibroglandular and adipose tissue

As mentioned above, over the last few years, with the benefit of dedicated breast CT, it has become apparent that previous breast dosimetry models on average result in an overestimation of the breast dose of approximately 30%.[15,16] This is a result of the tendency, in non-augmented breasts, of the fibroglandular tissue to be concentrated towards the center of the breast (i.e., away from the outer areas). Therefore, the aim of this breast modeling work was to produce a breast model that reflected this non-uniformity in the breast density throughout the breast volume.

The developed model, described in a previous publication by Fedon et al.,[24] is based on the analysis of the internal distribution of fibroglandular tissue in 88 women's breasts. In that work, the dedicated breast CT images of these breasts were automatically segmented into their three major tissue components (skin, adipose, and fibroglandular tissue), and their mechanical compression during both CC and MLO positioning for DM or DBT imaging was simulated using finite element methods.[25] The resulting distribution of the fibroglandular tissue in these compressed breasts was analyzed, and three probability distribution functions (PDFs) per view, one for each direction in 3D, were fit to the median mass density of this tissue across all breasts.

As can be seen in Figure 5, the analysis performed by Fedon et al demonstrates that the fibroglandular tissue does indeed tend to be concentrated away from the outer areas of the breast volume, with its highest density location somewhat below the vertical midline of the breast. This distribution in the axial (breast compression paddle to support table) direction is the main factor for the determination of the magnitude of the Γ in the breast. In the coronal (chest wall to nipple) direction, the distribution of the fibroglandular tissue can be seen to be quite uniform, with a considerable increase in density close to the nipple. Finally, in the sagittal (medial to lateral) direction, the fibroglandular tissue distribution is symmetric about the midline in the CC view breast, while the peak is somewhat offset in the MLO view compression.

These six functions were used to compose the distribution of adipose and fibroglandular tissue in the 286 breast phantoms listed in Table 4. This process is described in Caballo et al.[21] Given that the fibroglandular density throughout the internal breast tissue portion is non-uniform, obtaining the desired overall breast density based on these PDFs involved an optimization process. This is because above a certain overall density threshold, the voxels with the highest densities will be saturated by reaching a composition of 100% fibroglandular tissue content (Figure 6). However, this threshold does not set the maximum possible overall breast density. Rather, the rest of the internal breast volume should continue to get denser with increasing overall density, continuing to follow the distributions described by the PDF. Therefore, for breast models of higher density, the final tissue density distributions include a core of voxels containing 100% fibroglandular tissue with a smooth decrease in density outwards, as shown in Figure 6.

As described in Appendix C, the breast dose model developed here results in an average reduction of the breast dose estimate of approximately 30–40% when compared to defining the fibroglandular tissue as being uniformly distributed across the whole breast. Appendix C also includes comparisons of new dose estimates to those performed with previous models.

4.2.8 | Pectoral muscle

The pectoral muscle is included in an appropriately acquired MLO view DM or DBT image, and the dose absorbed by the muscle should not be included in the estimate of Γ. Therefore, an appropriate model of the MLO view breast should include a model of the muscle.

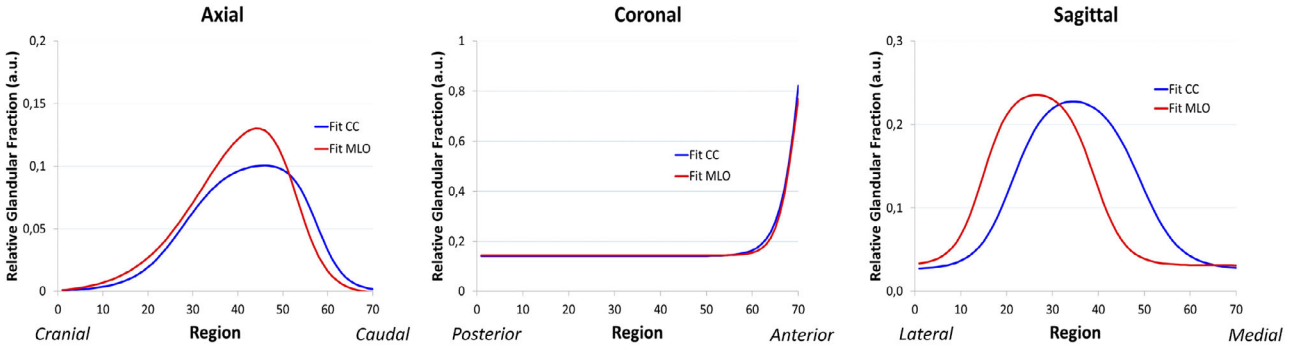

FIGURE 5 Fibroglandular tissue density distributions obtained from analysis of 88 dedicated breast CT images. Adapted from Fedon et al., Medical Physics, 2021; 48(3): 1436–1447.

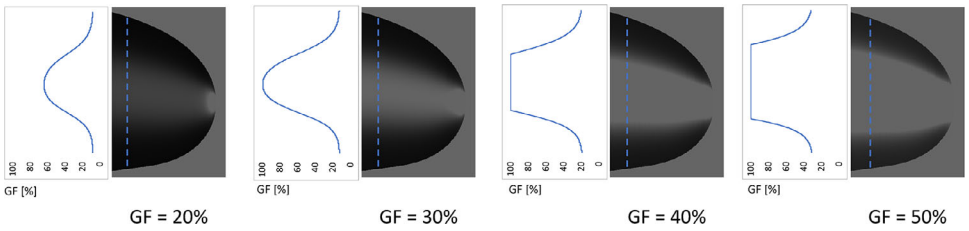

FIGURE 6 Example of voxel density saturation in high-density breast models and the resulting deviation in the density distribution from that given by the model probability distribution functions.

For this, a multi-step process was used to add a representation of the pectoral muscle to the MLO view breast model, as described by Caballo et al.[21] The muscle was defined as having the 2D shape in the midplane of that characterized by Rodriguez-Ruiz et al. in their analysis of 1000 DM images.[22] That is, the projected outline of the muscle is similar to a triangle, from the posterior edge of the image at the height of the nipple, getting wider towards the cranial edge of the image. In the direction between the compression paddle and the support table, the muscle was defined as positioned around the midplane of the breast, increasing in thickness symmetrically from the caudal to the cranial side (Figure 7).

Although the 2D shape of the projection of the pectoral muscle was easily characterized from DM images by Rodriguez-Ruiz et al.,[22] its thickness profile in the direction between the compression paddle and support table is challenging to characterize. The vertical resolution in DBT images is not sufficient to determine the variation in thickness of this structure throughout the image. Furthermore, the corresponding portion of the muscle is not included in most dedicated breast CT images, making its appearance in any form in the simulations of the compressed breast from segmented breast CT images unrealistic.

Given these limitations, a study was performed in which the sensitivity of the average glandular dose estimates to different muscle shapes was evaluated.[21] If a low enough sensitivity was found, then the lack of evidence in the modeling of this tissue structure would

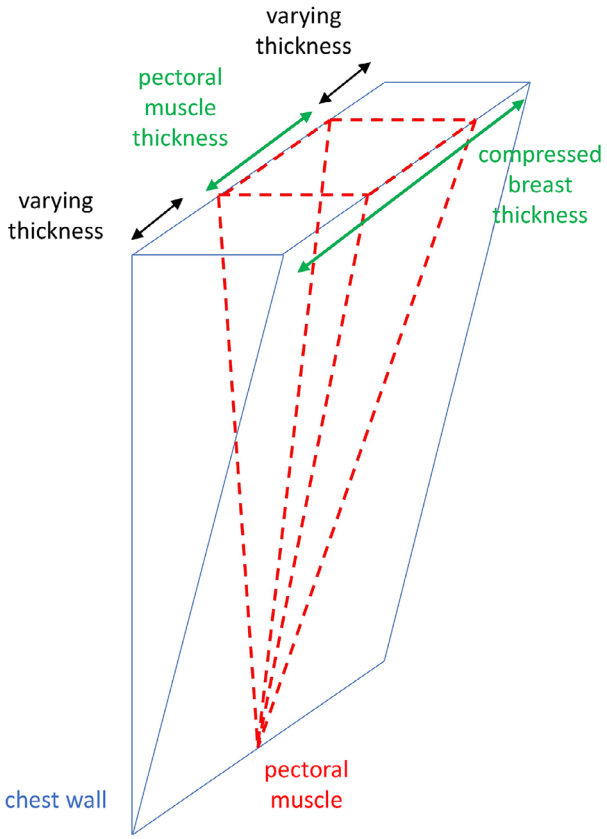

FIGURE 7 3D representation of the pectoral muscle solid included in the model of the breast in the MLO view. Adapted from Caballo et al., Medical Physics, 2022;49(8): 5423–5438.

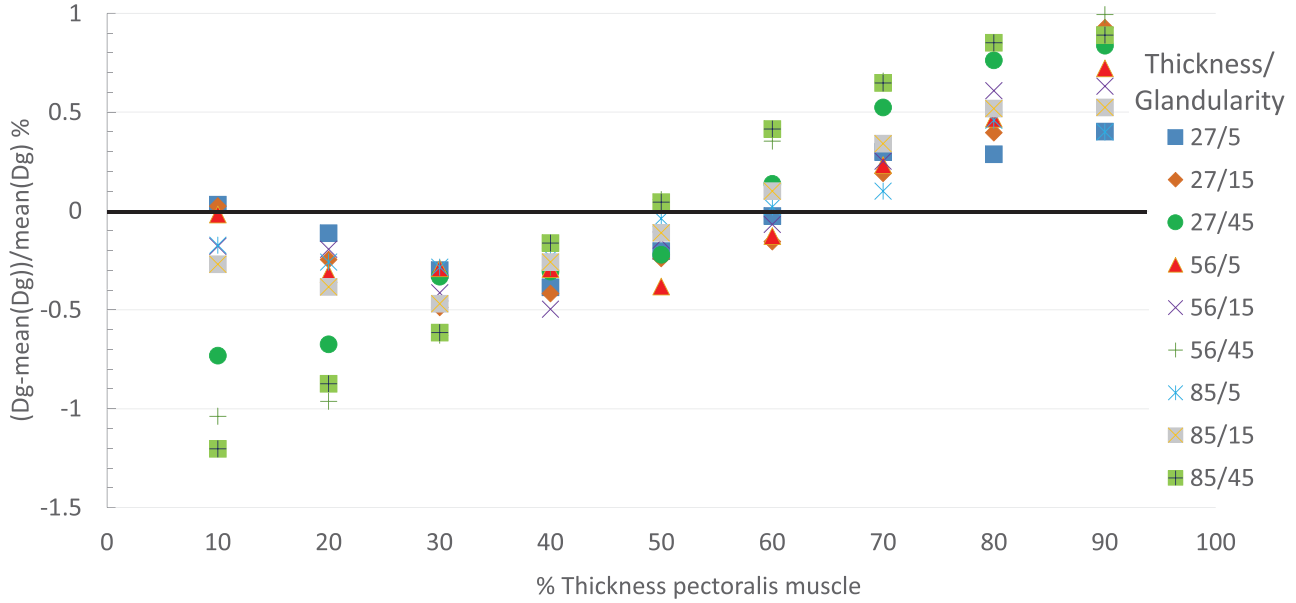

FIGURE 8 Deviations from the mean Γ estimates for 81 different phantoms with nine different breast thicknesses and densities. Each equal breast thickness and density set of phantoms is defined as having one of nine different pectoral muscle thickness profiles. The resulting Γ deviation estimates are normalized by the average Γ across muscle thickness profiles. The muscle thickness profile has a minimum impact on the dose estimates, with all deviations being smaller than 1.2% and most being less than 0.5%. The mean of one of the roots of each polynomial fit, 58%, was used as the final pectoral muscle relative thickness in the breast model for the MLO view. Adapted from Caballo et al, Medical Physics, 2022;49(8): 5423–5438.

not have a significant impact on the final Γ published in this report. The study involved generating MLO view breast phantoms with a range of compressed breast thicknesses, breast densities, and with pectoral muscles defined as having different thicknesses at the cranial edge of the phantom. The Γ for all these different phantoms was estimated using Monte Carlo simulations and its variation with muscle thickness profile characterized. As can be seen in Figure 8, the variation in average glandular dose with different definitions of the pectoral muscle thickness is minimal, with most deviations from the average being less than 0.5%.

As a result of further analysis, Caballo et al recommended that the final pectoral muscle model be defined as having a maximum thickness at the cranial edge of the MLO view image of 58% of that of the thickness of the internal breast tissue.[21]

Based on these developments, the final breast model used in this Report was used to generate the 286 different breast phantoms listed in Table 4 and used in the Monte Carlo simulations described in Section IV.D to obtain the estimated $\gamma_{sim}(t,\ g,\ e, a)$ used for this breast dosimetry method.

4.3 | X-ray field model

To obtain the dose conversion coefficients $\gamma_{sim}(t,\ g,\ e, a)$, Monte Carlo simulations of the DM/DBT/CEDM/CEDBT exposures using the breast phantoms generated as described in Section IV.A must be performed. Therefore, a model of these exposures was developed, with the parameters as listed in Table 5 and the geometry depicted in Figure 9.

4.3.1 | X-ray source and field shape

The x-ray source in the acquisition model was defined as a point source, located exactly above the chest wall edge of the breast and detector. The x-ray field emitted by the source at the 0° projection (equivalent to the DM/CEDM geometry) was 240 mm x 300 mm in area at the detector, and congruent with the detector limits. For non-zero projection angles, the short sides of the virtual collimation of the field were modified to maintain the congruence of the x-ray field in these two sides with the detector edges. The anterior side of the virtual collimation did not change with projection angle. This collimation behavior reflects many of the current DBT/CEDBT systems.

4.3.2 | X-ray intensity distribution

The x-ray intensity distribution incident upon the superior surface of the breast depends on the distance from each point to the x-ray source and on the heel effect. The variation due to these two effects was included in the specification of the x-ray beam for these simulations. To model them, the heel effect (and inherently the

TABLE 5 Characteristics of the image acquisition model for estimating the $\gamma_{sim}(t, g, e, a)$ for the four imaging modalities included in this breast dosimetry method.

Parameter	Unit	Values
Geometry parameters		
Source to support table distance	mm	648
Source to detector distance	mm	670
Air gap (including thickness of breast support)	mm	22
Source center of rotation to detector distance	mm	0
X-ray field size at detector	mm	240 × 300
Projection angular range	deg	-30°—+30°
Number of projections	–	21
System components		
Breast compression paddle thickness	mm	2.7
Breast compression paddle composition	–	Polycarbonate
Breast support table thickness	mm	2.0
Breast support table composition	–	Carbon Fiber
X-ray parameters		
Energy range	keV	9.75 – 48.75
Energy step size	keV	1.0

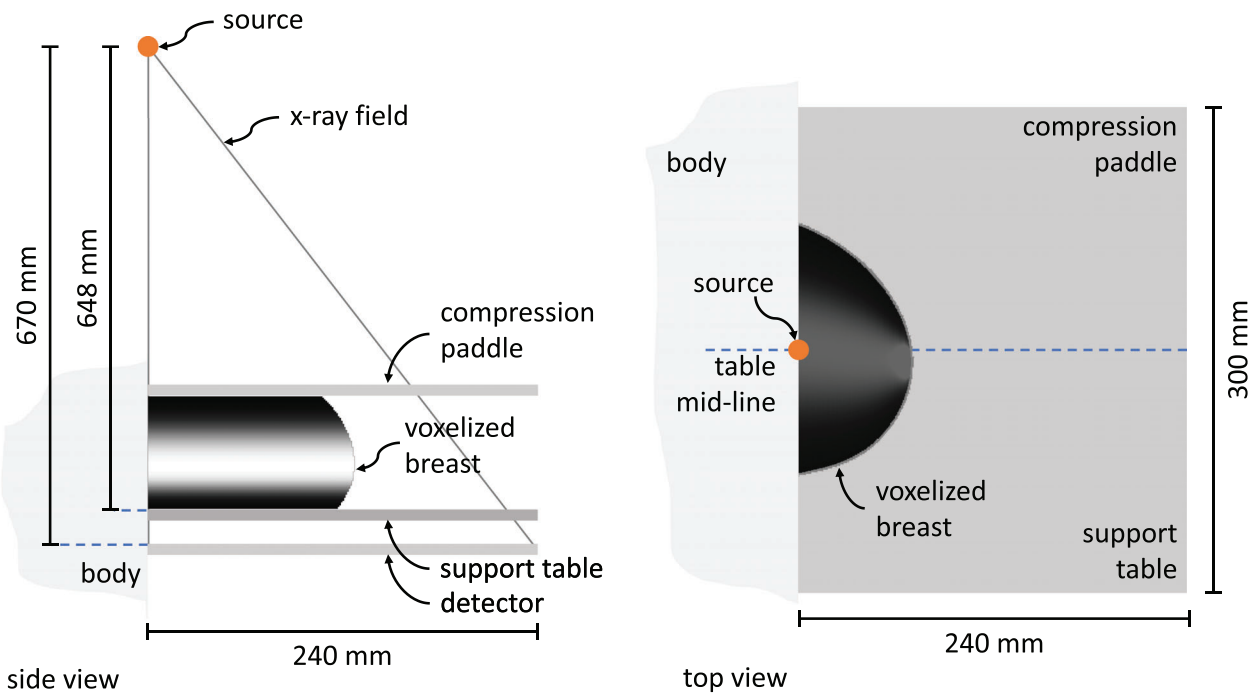

FIGURE 9 Schematics of the geometry defined as the acquisition model for the estimation of the $\gamma_{sim}(t, g, e, a)$ coefficients using Monte Carlo simulations. In these schematics, only the $a = 0°$ model is shown.

variation due to the inverse square law) of nine different imaging systems, comprising seven different system models from six different vendors including both DM and CEDM acquisitions, was characterized using physical measurements. In previous work, the independence of the variation in the incident air kerma in the chest wall-to-nipple direction from that in the direction along the chest wall had already been verified.[2] Therefore, for these nine system measurements, only the incident air kerma variations along the midline of the detector in the chest wall to nipple direction, and along the chest wall edge of the detector were measured. The measurements were performed with calibrated ionization chamber-based dosimeters, with the entrance surface of the chamber

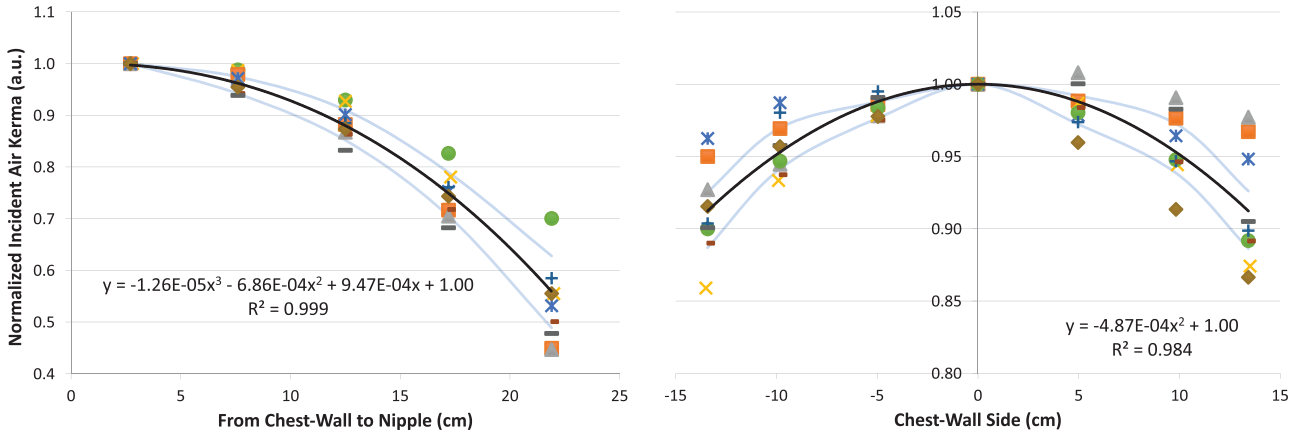

FIGURE 10 Results of measuring the impact of the heel effect and the distance from the source on the x-ray field of nine different DM, DBT, and CEDM imaging systems. For each perpendicular direction the average results in each position were fit to polynomial functions (black lines, with 95% confidence intervals in light blue) and used to define the emission of the x-ray field in the Monte Carlo simulations.

rotated as needed to face the source at each location. Figure 10 shows the graphs of the measured incident air kerma variations along the two measurement lines, and the functions fit to the average of these measured variations. The product of these two functions was used in the Monte Carlo simulations as the PDF for the direction of emission of the x-rays during the simulations.

Although there is an important dispersion in the magnitude of the heel effect across systems, the error introduced by this variability is expected to be minor. This is because it has been shown that the total impact of the presence of the heel effect on D_g estimates is 7%, compared to not including a heel effect at all.[2] Therefore, any variability in the heel effect that could be encountered in clinical systems must result in a considerably smaller error.

4.4 | Monte Carlo simulations

4.4.1 | Simulations

Two sets of Monte Carlo simulations were performed to estimate $\gamma_{sim}(t,\ g,\ e, a)$. The first involved the estimation of the energy deposited in the fibroglandular tissue portion of the breast models, $E_{g,MC}(t,\ g,\ e, a)$ as a result of certain exposure conditions. These simulations were performed for the breasts specified in Table 4 and the conditions specified in Table 5. The second set of simulations was to estimate the incident air kerma at the reference point, $K_{MC}(e)$ for those same exposure conditions, that is, those listed in Table 5, but only for the 0° projection angle.

All Monte Carlo simulations were performed with a previously developed and validated program based on the Geant4 toolkit, using the parameters listed in Table 6.

4.4.2 | Scored quantities

The first set of Monte Carlo simulations scored the energy deposited in the fibroglandular tissue portion of the breast voxels containing some percentage of fibroglandular tissue by the simulated 10^7 x-rays, denoted $E_{g,MC}$.

During the simulation, each interaction event i by an x-ray of energy ε that resulted in a deposition of energy $E_{dep,i}(g_{vox})$ in a voxel partially occupied by fibroglandular tissue with mass fraction g_{vox} was detected. Note that ε is not necessarily equal to e due to the x-ray potentially having already undergone an incoherent scatter event. The energy deposition was then weighted by the ratio of energy deposited in the fibroglandular portion of the voxel, and added to the running total of $E_{g,MC}$ using:

$$E_{g,MC} = \sum_i E_{dep,i}(g_{vox}) \frac{g_{vox}\left(\frac{\mu_{en}}{\rho}\right)_{gland}(\varepsilon)}{g_{vox}\left(\frac{\mu_{en}}{\rho}\right)_{gland}(\varepsilon) + (1-g_{vox})\left(\frac{\mu_{en}}{\rho}\right)_{adip}(\varepsilon)} \quad (8)$$

where $\left(\frac{\mu_{en}}{\rho}\right)_{gland}(\varepsilon)$ and $\left(\frac{\mu_{en}}{\rho}\right)_{adip}(\varepsilon)$ are the mass-energy absorption coefficients for fibroglandular and adipose tissue, respectively.

The second set of Monte Carlo simulations scored the air kerma at the reference point due to the simulated 10^7 x-rays, denoted K_{MC}. For this, during the simulation, the photon fluence in a 30 mm x 30 mm square area centered around the reference point was scored, and the air kerma

TABLE 6 Monte Carlo simulation parameters used to obtain $\gamma_{MC}(t,\ g,\ e, a)$ estimates.

Parameter	Description	Ref.
Code, version/release date	Geant4 toolkit (version 10.03, released December 2016)	26,27
Validation	Against Case 3 of AAPM TG Report 195[28] and against experimental dose measurements	29,30
Timing	e.g., 55 mm thick breast, 10% density, 20 keV x-rays: ~1300 s	
Source description	See Section IV.C	–
Cross-sections	EM standard option 4	–
Transport parameters	All cuts set to 1.0 mm, equivalent to 2.65 keV in 50% dense tissue	–
Variance reduction	None	–
Number of histories/statistical uncertainty	$E_{g,MC}$: 10^7 x-rays; maximum uncertainty < 0.7%. K_{MC}: 10^7 x-rays; maximum uncertainty < 0.8%.	
Statistical methods	Running uncertainty calculation	31

calculated using:

$$K_{MC} = \sum_i \frac{\varepsilon_i \left(\frac{\mu_{tr}}{\rho}\right)(\varepsilon_i)}{A\cos\theta_i} \tag{9}$$

where ε_i is the energy of the x-ray i crossing the scoring surface, $(\frac{\mu_{tr}}{\rho})(\varepsilon_i)$ is the mass-energy transfer coefficient in air for photons with energy ε, A is the area of the scoring surface, in this case, 900 mm^2, and θ_i is the incidence angle of x-ray i with the scoring surface.

As mentioned, this second set of simulations was only performed with the x-ray source at the 0° location, since all $\gamma_{MC}(t,\ g,\ e, a)$ coefficients are normalized by the reference air kerma with the x-ray source at that location, independent of the projection angle a. Furthermore, since K_{MC} is independent of the characteristics of the breast being exposed, the simulations did not have to be repeated for the various breasts listed in Table 4.

4.4.3 | Post-processing of Monte Carlo results

Upon termination of each Monte Carlo simulation that scored the energy deposited in the simulated breast, the average glandular dose was calculated by:

$$D_g\ (t,\ g,\ e, a) = \frac{E_{g,MC}}{m_g} \tag{10}$$

where m_g is the total mass of fibroglandular tissue in the simulated breast, obtained from:

$$m_g = V_{voxel} \sum_j \frac{g_{vox,j}}{\frac{g_{vox,j}}{\rho_{gland}} + \frac{1-g_{vox,j}}{\rho_{adip}}} \tag{11}$$

where V_{voxel} is the volume of each voxel, $g_{vox,j}$ is the mass fraction of fibroglandular tissue in voxel j, ρ_{gland} is the density of fibroglandular tissue, and ρ_{adip} is the density of adipose tissue. The $\gamma_{MC}(t,\ g,\ e, a)$ conversion coefficients were then computed using:

$$\gamma_{MC}\ (t,\ g,\ e, a) = \frac{D_g\,(t,\ g,\ e, a)}{K_{MC}\,(e)} \tag{12}$$

With Equation 12, the resulting average glandular dose values are normalized by the incident air kerma at the reference point, to obtain the conversion coefficients for each combination of values of compressed breast thickness, breast density, x-ray energy, and projection angle (i.e., t, g, e, and a, respectively) included in the Monte Carlo simulations.

The final computation step to obtain the $\gamma_{sim}(t,\ g,\ e, a)$ coefficients used by the dosimetry software involves the interpolation of $\gamma_{MC}(t,\ g,\ e, a)$ obtained by the Monte Carlo simulations in 1.0 keV x-ray energy steps by approximation to 0.5 keV steps. This is done to match the energy resolution of the XASMICS-based x-ray spectral models, and to denoise the Monte Carlo results further. This was performed by fitting the original $\gamma_{MC}(t,\ g,\ e, a)$ for the range of energies e to fourth-order splines using a least squares spline approximation, for each combination of values of compressed breast thickness, breast density, and projection angle (i.e., t, g, and a). The resulting $\gamma_{sim}(t,\ g,\ e, a)$ are the final product of this TG/WG dosimetry model.

4.5 | Dosimetry software processes

4.5.1 | Interpolation of conversion coefficients to input conditions

At runtime, the $\gamma_{sim}(t,\ g,\ e, a)$ are retrieved and used by the dosimetry software for any user-selected breast and exposure conditions that comply with the input parameters specified in Table 3. For this, first, the $\gamma(t,\ g,\ e, a)$ factors for all energies e, for the *specific*

input breast thickness t, breast density g, and projection angles a, are calculated from the neighboring retrieved $\gamma_{sim}(t,\ g,\ e, a)$ factors (which are available for the specific values of t, g, and a listed in Tables 4 and 5) using three successive cubic splines interpolations. The resulting $\gamma(t,\ g,\ e, a)$ are used to calculate the desired Γ and D_g as per Equations 1–5.

4.5.2 | Spectral conversion coefficients

To obtain the spectral dose conversion coefficients Γ the software uses the MASMICS/RASMICS/TASMICS models of x-ray spectra, from now on referred to as XASMICS,[32] to calculate ψ. These models describe the x-ray fluence output from an x-ray tube with a molybdenum, rhodium, or tungsten anode and include the inherent filtration. The output of the models is in units of photons/mm^2 in x-ray energy bins 0.5 keV in width, from 1.25 to 48.75 keV. These fluence outputs are simply multiplied by the corresponding x-ray energy to obtain the energy fluence ψ.

As mentioned above, the Monte Carlo simulations were performed only for the range from 9.75 to 48.75 keV, with the x-rays below this minimum deemed non-relevant for dosimetry estimates. Furthermore, as noted, the Monte Carlo simulations were performed in 1.0 keV steps, deeming these of sufficient resolution to obtain accurate dose estimates, and the resulting $\gamma(t,\ g,\ e, a)$ estimates interpolated to the energy step size that matches that of the XASMICS model.

Finally, the mass-transfer coefficients for air, $(\frac{\mu_{tr}}{\rho})_{air}(e)$ used are the ones distributed together with the XASMICS model. The rest of the parameters in Equation 6 are obtained from the user inputs, as described in Section III.D.

5 | KEY RECOMMENDATIONS

The following are the key recommendations of this joint TG/WG Report, the basis and rationale for them being included throughout the Report:

- The breast model used for dosimetry estimates should be based on fibroglandular density percentiles across the population, rather than on fixed percentage values.
- When referring to breast fibroglandular density, the metric to be used should be the volumetric breast density, defined as the volume of the entire breast, including the skin, that is occupied by fibroglandular tissue.
- When breast density is unknown (e.g., in the case of retrospective dose estimation for patient acquisitions) use the 50th percentile density corresponding to the patient compressed breast thickness, do not use 50% breast density.
- If estimating D_g for a compressed breast thickness below 15 mm or above 120 mm is needed, use the D_g estimate for a 15 or a 120 mm thick compressed breast, respectively.
- If estimating D_g for other non-standard views is needed, use the D_g estimate for the CC view.
- For prospective (i.e., phantom-based) testing, use the array of standard breasts.
- Use system-specific spectral models, allowing the software to adjust the model to the measured first HVL.
- The measurement of K_m should be performed using the collimation of the system that produces the largest x-ray field possible.
- During measurement of K_m, the breast compression paddle should be positioned as high as allowed by the system.
- Ensure that the dosimeter used to measure Km is backscatter insensitive, or measure Km free in air.

ACKNOWLEDGMENTS

The Task Group members would like to thank Naema Al-Maymani, Areej S Aloufi, Vanessa Atienza-Hipolito, Francis Hasford, Solveig Hofvind, Aanchal Kuckian, Shivaani Mariapun, Donald McLean, Stewart M. Midgley, Kartini Rahmat, Rasika Rajapakshe, Silje Sagstad, Jothy Selvaraj, Soo-Hwang Teo, Alessandra Tomal, Athina Vourtsis, Wen-pei Wu, and the OPTIMAM Mammography Image Database funded by Cancer Research UK (C30682/A28396) for providing the population breast density datasets used in this Report; Kim Lemmens, Anne Bolderdijk, and Onno van der Helm for contributing with measurements of the heel effect in various digital mammography systems; Tushita Patel, Andrew Smith, Steffen Kappler, Stefan Veitenhansl, Julia Wicklein, Razvan Iordache, Remy Klausz, Serge Muller, Takao Kuwabara, Joerg Mueller, and Robert Uzenoff for providing feedback and input throughout the entire process; John Loveland and the Scientific Computing Section of the Royal Surrey, Guildford, UK, for providing feedback and testing of the software code and for hosting the web-based version of the dosimetry program; and Kris Modrak for developing the software interfaces. [Correction added on 6 December, 2023 after first online publication: Acknowledgment section is updated.]

CONFLICT OF INTEREST STATEMENT

1. The members of the Joint AAPM Task Group 282/EFOMP Working Group for the development of a new universal breast dosimetry method listed below attest that they have no potential Conflicts of Interest related to the subject matter or materials presented in this document.

David R. Dance
Marco Caballo

Oliver Diaz
Ruben van Engen
Christian Fedon
Stephen J. Glick
Katie W. Hulme
Renata Longo
Carolina Rabin
Wendelien B.G. Sanderink
J. Anthony Seibert

2. The members of the Joint AAPM Task Group 282/EFOMP Working Group for the development of a new universal breast dosimetry method listed below disclose the following potential Conflict(s) of Interest related to subject matter or materials presented in this document.

Ioannis Sechopoulos: Research agreements, Canon Medical Systems, Siemens Healthcare, ScreenPoint Medical, Sectra Benelux, Volpara Health, Lunit, iCAD, Siemens Healthcare. Scientific Advisory Board, Koning Corporation.

John M. Boone: Cofounder, Director, and Shareholder, Izotropic Imaging Corporation.

Hilde T. Bosmans: Co-owner, Qaelum NV and Qaelum Inc.

Andrew M. Hernandez: Consultant, Izotropic Imaging Corporation.

Melissa L. Hill: Consultant, Volpara Health. Scientific Advisory Board, MVG Industries.

The Chair of the Joint AAPM Task Group 282/EFOMP Working Group for the development of a new universal breast dosimetry method has reviewed the required Conflict of Interest statement on file for each member of the Joint AAPM Task Group 282/EFOMP Working Group for the development of a new universal breast dosimetry method and determined that disclosure of potential Conflicts of Interest is an adequate management plan. Disclosures of potential Conflicts of Interest for each member of the Joint AAPM Task Group 282/EFOMP Working Group for the development of a new universal breast dosimetry method are found at the close of this document.

ORCID

Ioannis Sechopoulos
https://orcid.org/0000-0001-9615-8205

REFERENCES

1. Dance DR, Sechopoulos I. Dosimetry in x-ray-based breast imaging. *Phys Med Biol*. 2016;61(19):R271-R304. doi:10.1088/0031-9155/61/19/R271
2. Sechopoulos I, Suryanarayanan S, Vedantham S, D'Orsi C, Karellas A. Computation of the glandular radiation dose in digital tomosynthesis of the breast. *Med Phys*. 2007;34(1):221-232. doi:10.1118/1.2400836
3. Dance DR. Monte Carlo calculation of conversion factors for the estimation of mean glandular breast dose. *Phys Med Biol*. 1990;35(9):1211-1219.
4. Wu X, Barnes GT, Tucker DM. Spectral dependence of glandular tissue dose in screen-film mammography. *Radiology*. 1991;179(1):143-148.
5. Wu X, Gingold EL, Barnes GT, Tucker DM. Normalized average glandular dose in molybdenum target-rhodium filter and rhodium target-rhodium filter mammography. *Radiology*. 1994;193(1):83-89.
6. Boone JM. Glandular breast dose for monoenergetic and high-energy X-ray beams: monte Carlo assessment. *Radiology*. 1999;213(1):23-37.
7. Dance DR, Skinner CL, Young KC, Beckett JR, Kotre CJ. Additional factors for the estimation of mean glandular breast dose using the UK mammography dosimetry protocol. *Phys Med Biol*. 2000;45(11):3225-3240.
8. Dance DR, Young KC, van EngenRE. Further factors for the estimation of mean glandular dose using the United Kingdom, European and IAEA breast dosimetry protocols. *Phys Med Biol*. 2009;54(14):4361-4372.
9. Dance DR, Young KC, van EngenRE. Estimation of mean glandular dose for breast tomosynthesis: factors for use with the UK, European and IAEA breast dosimetry protocols. *Phys Med Biol*. 2011;56(2):453.
10. Nosratieh A, Hernandez A, Shen SZ, Yaffe MJ, Seibert JA, Boone JM. Mean glandular dose coefficients (D g N) for x-ray spectra used in contemporary breast imaging systems. *Phys Med Biol*. 2015;60(18):7179.
11. Huang SY, Boone JM, Yang K, Kwan ALC, Packard NJ. The effect of skin thickness determined using breast CT on mammographic dosimetry. *Med Phys*. 2008;35(4):1199-1206.
12. Huang SY, Boone JM, Yang K, et al. The characterization of breast anatomical metrics using dedicated breast CT. *Med Phys*. 2011;38(4):2180-2191. doi:10.1118/1.3567147
13. Yaffe MJ, Boone JM, Packard N, et al. The myth of the 50-50 breast. *Med Phys*. 2009;36(12):5437-5443. doi:10.1118/1.3250863
14. Hammerstein GR, Miller DW, White DR, Masterson ME, Woodard HQ, Laughlin JS. Absorbed radiation dose in mammography. *Radiology*. 1979;130(2):485-491.
15. Sechopoulos I, Bliznakova K, Qin X, Fei B, Feng SSJ. Characterization of the homogeneous tissue mixture approximation in breast imaging dosimetry. *Med Phys*. 2012;39(8):5050-5059. doi:10.1118/1.4737025
16. Hernandez AM, Seibert AJ, Boone JM. Breast dose in mammography is about 30% lower when realistic heterogeneous glandular distributions are considered. *Med Phys*. 2015;42(11):6337-6348. doi:10.1118/1.4931966
17. National Research Council (U. S.). *Committee to Assess Health Risks from Exposure to Low Level of Ionizing Radiation*. Health Risks from Exposure to Low Levels of Ionizing Radiation : BEIR VII Phase 2. National Academies Press; 2006.
18. Sechopoulos I, Feng SSJ, D'Orsi CJ. Dosimetric characterization of a dedicated breast computed tomography clinical prototype. *Med Phys*. 2010;37(8):4110-4120. doi:10.1118/1.3457331
19. Sarno A, Dance DR, van Engen RE, et al. A Monte Carlo model for mean glandular dose evaluation in spot compression mammography. *Med Phys*. 2017;44(7):3848-3860. doi:10.1002/mp.12339
20. Zuley ML, Bandos AI, Ganott MA, et al. Digital breast tomosynthesis versus supplemental diagnostic mammographic views for evaluation of noncalcified breast lesions. *Radiology*. 2013;266(1):89-95. doi:10.1148/radiol.12120552
21. Caballo M, Rabin C, Fedon C, et al. Patient-derived heterogeneous breast phantoms for advanced dosimetry in mammography and tomosynthesis. *Med Phys*. 2022;49(8):5423-5438. doi:10.1002/mp.15785

22. Rodríguez-Ruiz A, Feng SSJ, van Zelst J, et al. Improvements of an objective model of compressed breasts undergoing mammography: generation and characterization of breast shapes. *Med Phys*. 2017;44(6):2161-2172. doi:10.1002/mp.12186
23. Rodríguez-Ruiz A, Agasthya GA, Sechopoulos I. The compressed breast during mammography and breast tomosynthesis: in vivo shape characterization and modeling. *Phys Med Biol*. 2017;62(17):6920-6937.
24. Fedon C, Caballo M, García E, et al. Fibroglandular tissue distribution in the breast during mammography and tomosynthesis based on breast CT data: a patient-based characterization of the breast parenchyma. *Med Phys*. 2021;48(3):1436-1447. doi:10.1002/mp.14716
25. García E, Fedon C, Caballo M, Martí R, Sechopoulos I, Diaz O. Realistic compressed breast phantoms for medical physics applications. *15th International Workshop on Breast Imaging (IWBI2020)*. International Society for Optics and Photonics; 2020:1151304. doi:10.1117/12.2564273
26. Agostinelli S, Allison J, Amako K, et al. Geant4 - A simulation toolkit. *Nucl Instrum Methods Phys Res Sect Accel Spectrometers Detect Assoc Equip*. 2003;506(3):250-303. doi:10.1016/S0168-9002(03)01368-8
27. Allison J, Amako K, Apostolakis J, et al. Geant4 developments and applications. *IEEE Trans Nucl Sci*. 2006;53(1):270-278.
28. Sechopoulos I, Ali ESM, Badal A, et al. Monte Carlo reference data sets for imaging research: executive summary of the report of AAPM Research Committee Task Group 195. *Med Phys*. 2015;42(10):5679-5691. doi:10.1118/1.4928676
29. Fedon C, Caballo M, Longo R, Trianni A, Sechopoulos I. Internal breast dosimetry in mammography: experimental methods and Monte Carlo validation with a monoenergetic x-ray beam. *Med Phys*. 2018;45(4):1724-1737. doi:10.1002/mp.12792
30. Fedon C, Caballo M, Sechopoulos I. Internal breast dosimetry in mammography: monte Carlo validation in homogeneous and anthropomorphic breast phantoms with a clinical mammography system. *Med Phys*. 2018;45(8):3950-3961. doi:10.1002/mp.13069
31. Sempau J, Sánchez-Reyes A, Salvat F, HO ben Tahar, Jiang SB, Fernández-Varea JM. Monte Carlo simulation of electron beams from an accelerator head using PENELOPE. *Phys Med Biol*. 2001;46(4):1163-1186. doi:10.1088/0031-9155/46/4/318
32. Hernandez AM, Seibert JA, Nosratieh A, Boone JM. Generation and analysis of clinically relevant breast imaging x-ray spectra. *Med Phys*. 2017;44(6):2148-2160. doi:10.1002/mp.12222
33. Morrish OWE, Tucker L, Black R, Willsher P, Duffy SW, Gilbert FJ. Mammographic breast density: comparison of methods for quantitative evaluation. *Radiology*. 2015;275(2):356-365. doi:10.1148/radiol.14141508
34. Moshina N, Roman M, Waade GG, Sebuødegård S, Ursin G, Hofvind S. Breast compression parameters and mammographic density in the Norwegian Breast Cancer Screening Programme. *Eur Radiol*. 2018;28(4):1662-1672. doi:10.1007/s00330-017-5104-5
35. Rahbar K, Gubern-Merida A, Patrie JT, Harvey JA. Automated volumetric mammographic breast density measurements may underestimate percent breast density for high-density breasts. *Acad Radiol*. 2017;24(12):1561-1569. doi:10.1016/j.acra.2017.06.002
36. Wang J, Azziz A, Fan B, et al. Agreement of mammographic measures of volumetric breast density to MRI. *PLoS One*. 2013;8(12):e81653. doi:10.1371/journal.pone.0081653

How to cite this article: Sechopoulos I, Dance DR, Boone JM, et al. Joint AAPM Task Group 282/EFOMP Working Group Report: Breast dosimetry for standard and contrast-enhanced mammography and breast tomosynthesis. *Med. Phys*. 2024;51:712–739. https://doi.org/10.1002/mp.16842

APPENDIX A: DERIVATION OF CORRECTION FACTOR FOR RECOMMENDED MEASUREMENT SETUP

As described in Section III.B, although D_g estimation is to be based on K_{ref}, the measurement of K_m is recommended for convenience. However, beyond the inverse square distance relationship, it can be expected that these two incident air kerma values differ due to the x-ray scatter from the compression paddle, among other minor factors. This is because the reference point is located closer to the compression paddle than the measurement point and, therefore, is affected by a higher amount of x-ray scatter from the paddle. To address this disparity, an empirical correction factor, c_k, is included in the dosimetry calculation software that increases K_m by 3.2%, in addition to performing the inverse square distance correction based on the input l_m. The correction factor, c_k, was defined as:

$$c_k = \frac{K_{ref}}{K_m}\left(\frac{500\ mm}{l_m}\right)^2 \quad \text{(A1)}$$

so that the correct value for K_{ref} can be arrived at from K_m by Equation 2.

To arrive at the value of c_k, a survey involving the measurement of K_m and K_{ref} across multiple mammography systems of different models from various manufacturers, using both solid-state- and ion-chamber-based dosimeters, at varying tube voltages, and where possible with different x-ray tube anodes and filters, was undertaken. In total, 128 measurements were performed, on 28 systems, involving ten different models from five different manufacturers, at over a dozen sites. The median of the 128 individual c_k values obtained according to Equation A1 was found to be 1.032 (range = [0.985, 1.069], $25^{th}/75^{th}$ percentiles = [1.017, 1.045], Figure A.1), and hence the value set for c_k in the breast dosimetry software for Equation 2 was 1.032.

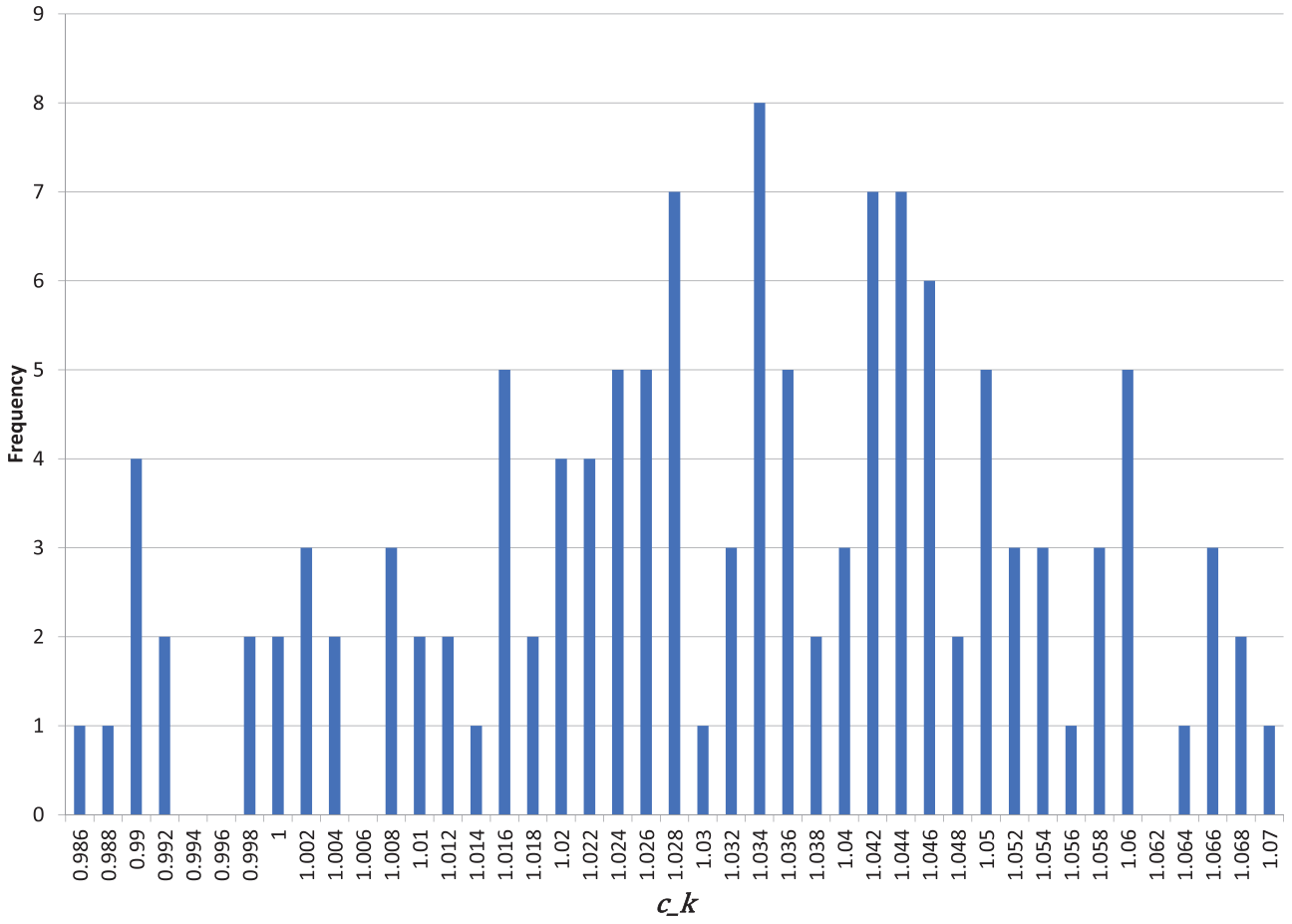

FIGURE A.1 Histogram of the c_k values obtained from 128 measurements on 28 different imaging systems. The median of the measurements is 1.032 (range = [0.985, 1.069], $25^{th}/75^{th}$ percentiles = [1.017, 1.045]), and hence the value set for c_k in the breast dosimetry software for Equation 2 is 1.032.

APPENDIX B: POPULATION BREAST DENSITY DISTRIBUTION

To estimate the relationship between breast density percentiles and percentages for different compressed breast thicknesses, a retrospective survey of volumetric breast densities from digital mammograms acquired in various countries around the world was performed. The inclusion criteria involved four-view digital mammography screening cases of women 50 years old or above. If a case included more than four views, then it was excluded since this might be associated with unsatisfactory positioning. All cases of repeated women attending screening over multiple rounds were included. Volpara Density was used on all images of all cases to estimate the volumetric breast density present in each mammogram. The "for processing" digital mammograms had to be available for analysis by the software, or the analysis could have been already performed at the source and only the results made available. For each case, an anonymized exam ID, age, side, view, compressed breast thickness, and volumetric breast density were obtained. In the case of datasets that could not include the individual age information due to anonymization regulations, the datasets included only data for women age 50 years old or above. A volumetric breast density per view for each case was calculated by averaging the value obtained for each side, and all analysis was performed separately for each view.

In total, data from 4 507 108 screening digital mammography images were collected and included in the analysis, from ten different datasets from as many countries, according to the breakdown in Table B.1.

The volumetric breast densities for each view were grouped in bins of 10 mm in compressed breast thickness, starting at 16 mm, up to 95 mm. From each of these eight thickness and two view bins, the 5^{th}, 25^{th}, 50^{th}, 75^{th}, and 95^{th} percentiles of VBD were estimated using SPSS software version 25 (SPSS Inc., Chicago, Illinois, USA), including an estimation of the 95% confidence intervals for each percentile estimate, via bootstrapping 1,000 times. Due to the low prevalence of compressed breasts with thicknesses below 16 mm and above 95 mm, it was not possible

TABLE B.1 Listing of countries and dataset size obtained for the population breast density distribution analysis that resulted in the standard breast model.

Country	Images	Cases	Women
Norway	2 190 110	548 012	206 953
Canada	816 450	204 142	
USA	743 998	189 859	
United Kingdom	282 724	71 018	70 848
Taiwan	251 192	65 094	50 831
Netherlands	130 786	32 780	30 916
Australia	46 960	11 740	11 740
Brazil	25 148	6402	5879
Greece	11 278	2873	2393
Malaysia	8462	2122	2121
Total	4 507 108	1 134 042	381 681

Note: The datasets from Canada and the USA did not include individual identifiers so as to be able to calculate the number of distinct women.

to estimate the density percentiles for the thicknesses ranges below and above these thresholds. Therefore, density percentiles for 15 mm and for 96–120 mm breast thicknesses could not be estimated directly from the data obtained. To obtain a model for the complete range of breast thicknesses included in the population-based model, the density percentiles for the closest thickness bin are used for these missing thicknesses.

Tables B.2 and B.3 list the resulting percentage densities for the five density percentiles and the eight compressed breast thicknesses that comprise the standard breast model. This data is also shown in Figures B.1 and B.2, which also include the corresponding 95% confidence intervals for each estimate. The larger differences observed for the higher percentiles are anticipated due to the known asymmetric nature of population breast density distributions, which exhibit long tails towards higher densities.[13]

The analysis of the population distribution of densities within specific compressed breast thicknesses, and therefore the resulting model, has several limitations. In the first place, it is impossible to include women from all different ethnicities or countries of the world in the analysis. A very substantial effort was made to be as inclusive as possible, but the availability of digital mammography data worldwide is limited, especially in numbers large enough to be able to provide

TABLE B.2 Volumetric breast densities, in percentages, and corresponding 95% confidence intervals, used by the standard population-based breast model for the CC view breasts, including the nearest-neighbor extrapolations to complete the model.

Compressed breast thickness (mm)	Volumetric breast density (percentile)				
	5th	25th	50th	75th	95th
15-25	10 (8.6-10.8)	14 (13.0-15.1)	18 (16.4-18.6)	22 (20.5-22.7)	28 (26.6-28.7)
26-35	7 (5.7-7.9)	10 (9.2-11.4)	14 (13.0-15.3)	19 (18.0-20.1)	26 (24.9-27.1)
36-45	5 (3.6-5.8)	7 (6.0-8.2)	10 (8.7-11.0)	14 (13.3-15.4)	23 (22.1-24.3)
46-55	4 (2.6-4.8)	5 (4.1-6.3)	7 (6.1-8.3)	10 (9.3-11.5)	19 (17.6-19.8)
56-65	3 (2.0-4.2)	4 (3.0-5.2)	5 (4.4-6.6)	8 (6.7-8.9)	13 (12.2-14.4)
66-75	3 (1.7-3.8)	4 (2.5-4.7)	5 (3.5-5.7)	6 (5.3-7.5)	11 (10.0-12.2)
76-85	2 (1.3-3.6)	3 (2.1-4.4)	4 (3.1-5.3)	5 (4.3-6.6)	10 (8.5-10.8)
86-95	2 (1.2-3.8)	3 (1.9-4.5)	4 (2.8-5.4)	5 (4.2-6.8)	10 (8.6-11.2)
96-120	2 (1.2-3.8)	3 (1.9-4.5)	4 (2.8-5.4)	5 (4.2-6.8)	10 (8.6-11.2)

TABLE B.3 Volumetric breast densities, in percentages, and corresponding 95% confidence intervals, used by the standard population-based breast model for the MLO view breasts, including the nearest-neighbor extrapolations to complete the model.

Compressed breast thickness (mm)	Volumetric breast density (percentile)				
	5th	25th	50th	75th	95th
15-25	10 (8.6-10.5)	13 (12.1-14.0)	17 (15.7-17.6)	21 (19.7-21.6)	28 (26.7-28.6)
26-35	7 (6.3-8.1)	10 (9.5-11.3)	14 (12.9-14.7)	19 (17.6-19.4)	25 (24.2-26.0)
36-45	5 (4.2-6.0)	7 (6.6-8.4)	10 (9.4-11.2)	14 (13.6-15.4)	22 (21.4-23.2)
46-55	4 (3.0-4.8)	6 (4.6-6.4)	7 (6.6-8.4)	11 (9.8-11.6)	18 (17.2-19.0)
56-65	3 (2.3-4.1)	4 (3.4-5.2)	6 (4.8-6.6)	8 (7.1-8.9)	13 (12.5-14.3)
66-75	2 (1.8-3.6)	3 (2.7-4.5)	5 (3.8-5.6)	6 (5.5-7.3)	11 (9.7-11.5)
76-85	2 (1.5-3.4)	3 (2.3-4.1)	4 (3.2-5.0)	5 (4.5-6.3)	9 (8.0-9.9)
86-95	2 (1.3-3.2)	3 (1.9-3.8)	4 (2.6-4.5)	5 (3.7-5.6)	8 (7.1-9.0)
96-120	2.3 (1.3-3.2)	2.8 (1.9-3.8)	4 (2.6-4.5)	5 (3.7-5.6)	8 (7.1-9.0)

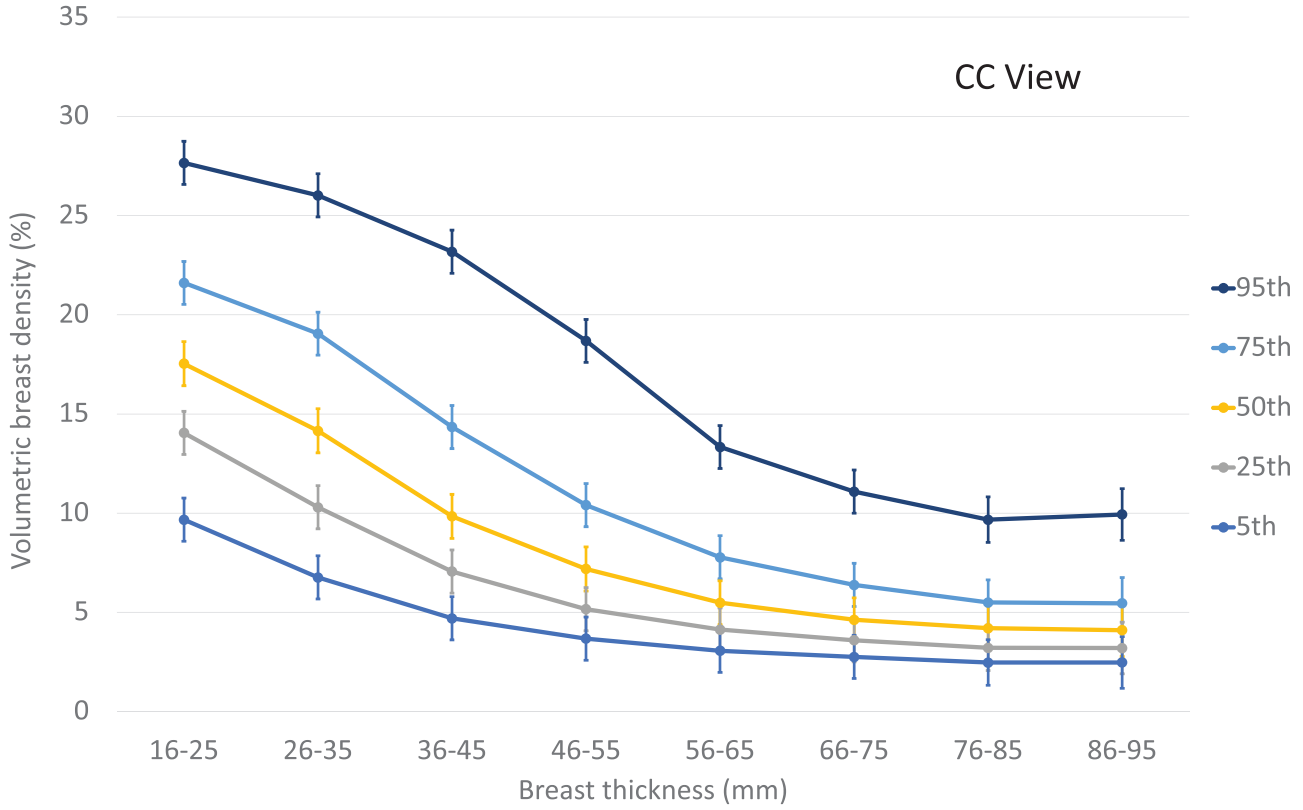

FIGURE B.1 Resulting volumetric breast densities, in percentages, and corresponding 95% confidence intervals, from the population density distribution analysis for the CC view breasts.

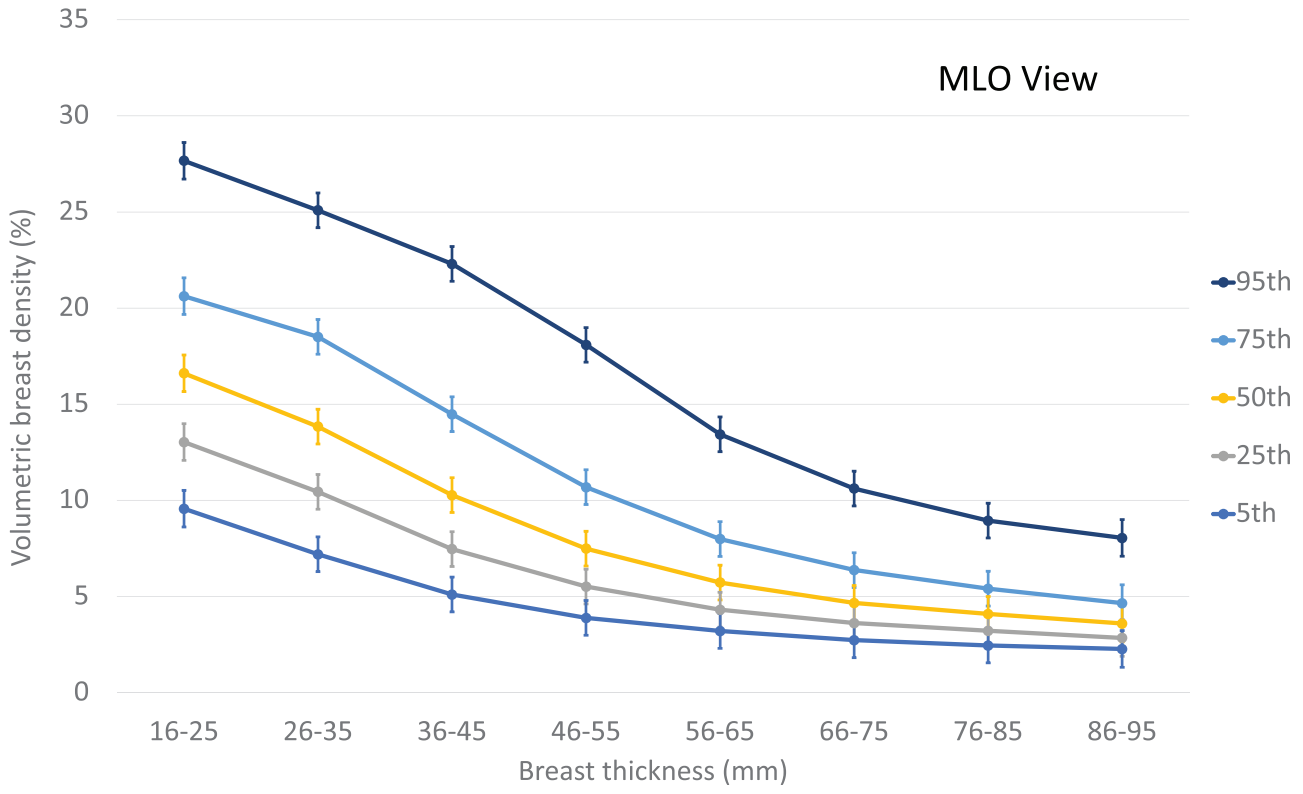

FIGURE B.2 Resulting volumetric breast densities, in percentages, and corresponding 95% confidence intervals, from the population density distribution analysis for the MLO view breasts.

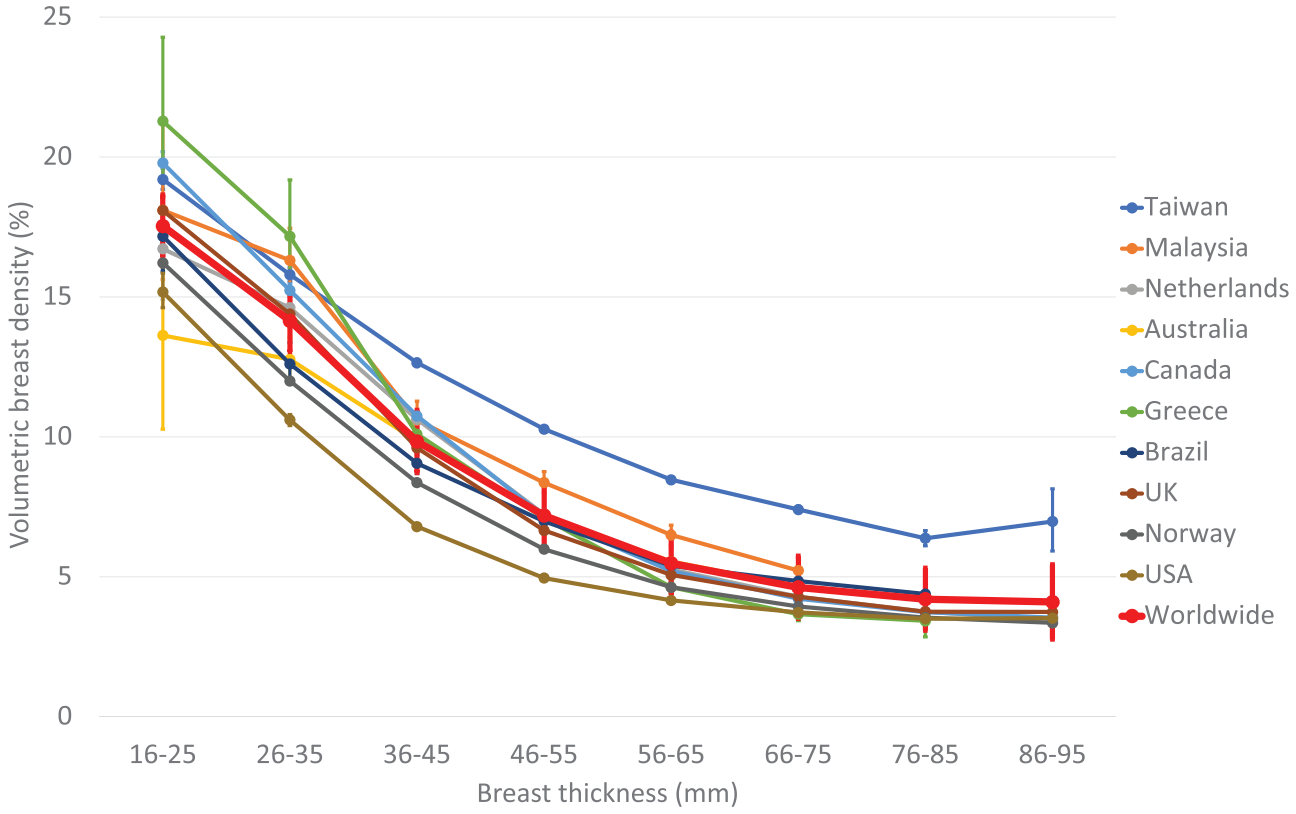

FIGURE B.3 50th percentile CC-view volumetric breast densities (VBDs) estimated for each of the ten different datasets obtained for the development of the breast model and for the resulting single worldwide model. Although the values diverge from the model ones for some regions, the impact of the differences is minor, as can be seen in Table B.4. Missing data points are due to lack of data in the original datasets.

meaningful data when divided per breast density and compressed breast thickness. This limitation is compounded by the need to have "for processing" images available, which are routinely not saved after a few weeks post acquisition, or for those images to have been already analyzed with density estimation software. Therefore, if the distribution of breast densities within each bin of compressed breast thickness varies around the world due to different ethnicities, this is not considered. In any case, if country of origin or ethnicity were to be considered in the model, then the standard breast model used in each country would have to be different, introducing a lack of consistency throughout different countries.

To gauge the additional variability in the relationship between density percentiles and percentages that could be introduced due to variations in country of origin, an explanatory model analysis was performed on the data available. This involved analyzing the data with an explanatory model based on general linear models. This analysis showed that the country of origin explained 10.1% and 7.3% of the variance seen in the data for CC and MLO projections respectively.

To depict the impact of this variance not being considered in the model, as an example, Figure B.3 shows the 50th percentile volumetric breast densities for the CC view estimated for each of the 10 different datasets and the global model, including the corresponding 95th percentile confidence intervals. In addition, Table B.4 shows the six specific conditions that have the largest positive or negative divergence from the global estimate for the 5th, 50th, and 95th percentile densities, and the resulting difference in Γ, and therefore, the differences that would result in the estimated average glandular dose. As can be seen, the simplification of using a single breast density model worldwide as opposed to one per country or region, introduces errors in the dose estimates of mostly $< 3\%$, and, in one case, of 5.6%. Therefore, clearly, in addition to the challenge of obtaining enough data to develop country- or region-specific models, the added effort of attempting to use the correct model for each dose estimate individually seems unjustified.

As shown in Tables B.2 and B.3 and the corresponding graphs, the volumetric breast density of the population datasets is overall low, with values that could seem low compared to prior breast densities used or assumed for dosimetry estimates. However, it is important to point out two differences between these values and those previously used.

TABLE B.4 Example estimates of dose conversion coefficients, Γ, for different breasts when using the single worldwide breast model to define the density of the breast versus using the value obtained for the corresponding region.

			Worldwide model		Region-specific model		
Region	Percentile breast density	Breast thickness (mm)	Volumetric breast density (%)	Dose conversion coefficient (mGy/mGy)	Volumetric breast density (%)	Dose conversion coefficient (mGy/mGy)	% difference Dose
USA	5th	40	5	0.174	3	0.175	−0.6%
Taiwan	5th	90	2	0.078	4	0.077	1.3%
USA	50th	50	7	0.143	5	0.145	−1.4%
Taiwan	50th	90	4	0.077	7	0.077	0.0%
Netherlands	95th	90	10	0.075	7	0.077	−2.6%
USA	95th	90	10	0.075	15	0.071	5.6%

The spectra assumed for the dose estimates were those selected by the automatic exposure control of a clinical digital mammography system.

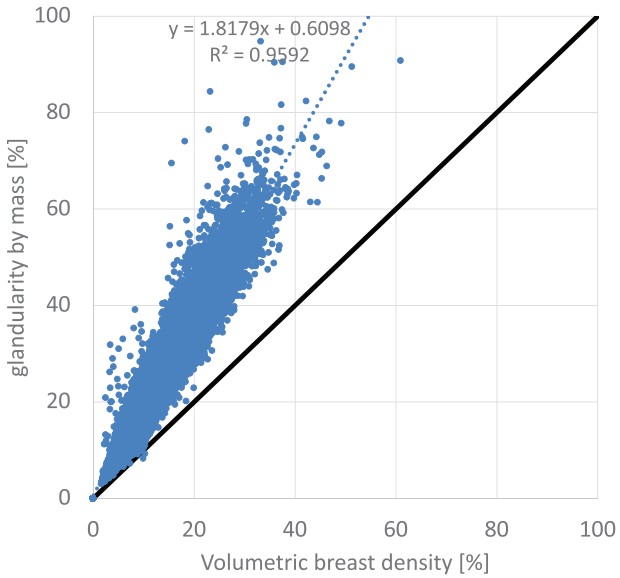

FIGURE B.4 Comparison between breast glandularity by mass and volumetric breast density for a sample of 152 137 screening digital mammograms, and their corresponding summary statistics, showing the difference in magnitude between these two metrics and the differences reflected between the mean and the median.

In the first place, breast dosimetry methods until now have, for the most part, used breast density by mass rather than by volume. As discussed above, this differs from the density metric used by most clinical density quantization algorithms, and it is advantageous to be consistent across these two different applications. In addition, it is common for breast density distributions to be summarized using the mean rather than the median, even though the distributions are not normal. Figure B.4 shows the distribution of volumetric breast density and breast density by mass for the entire Dutch dataset listed in Table B.1. As can be seen, breast density values are considerably higher when evaluated by mass rather than by volume. In addition, the medians of population breast density distributions are also lower than their means. Therefore, with these two effects combined, as in this example, a population mean density by mass of about 14% actually reflects a distribution with a median volumetric breast density of only 6%.

It should also be noted that some breast density quantifications evaluate area breast density as opposed to volumetric. Morrish et al has shown that area-based breast density evaluations also results in higher breast density values than those describing volumetric breast density.[33]

When considering distributions of volumetric breast density estimates and equivalent summary values, various prior publications have shown ranges and values comparable to those used here for the population-based breast model.[33,34] In addition, and importantly, prior publications have also shown that the breast density quantification software used for this Report results in values comparable to those from other algorithms,[33,35] although some other studies have found important deviations, but usually with lower number of patients.[36]

APPENDIX C: DIFFERENCES BETWEEN AVERAGE GLANDULAR DOSE ESTIMATES WITH THIS MODEL VS. PREVIOUS MODELS

To compare the estimates of average breast glandular dose of this new method to those obtained with prior existing methods, large datasets of acquisition techniques of digital mammography of patients or screened women were retrieved. The information retrieved for each of these acquisitions was the imaging system used, mammographic view, compressed breast thickness, target/filter combination, tube voltage, 1st half value layer, the incident air kerma, and the average glandular dose estimate. For the new method, the source-to-breast support table distance was also obtained for each imaging system in question. In addition, as recommended in this Report, the volumetric breast density for each record was set to the 50th percentile density (for that compressed

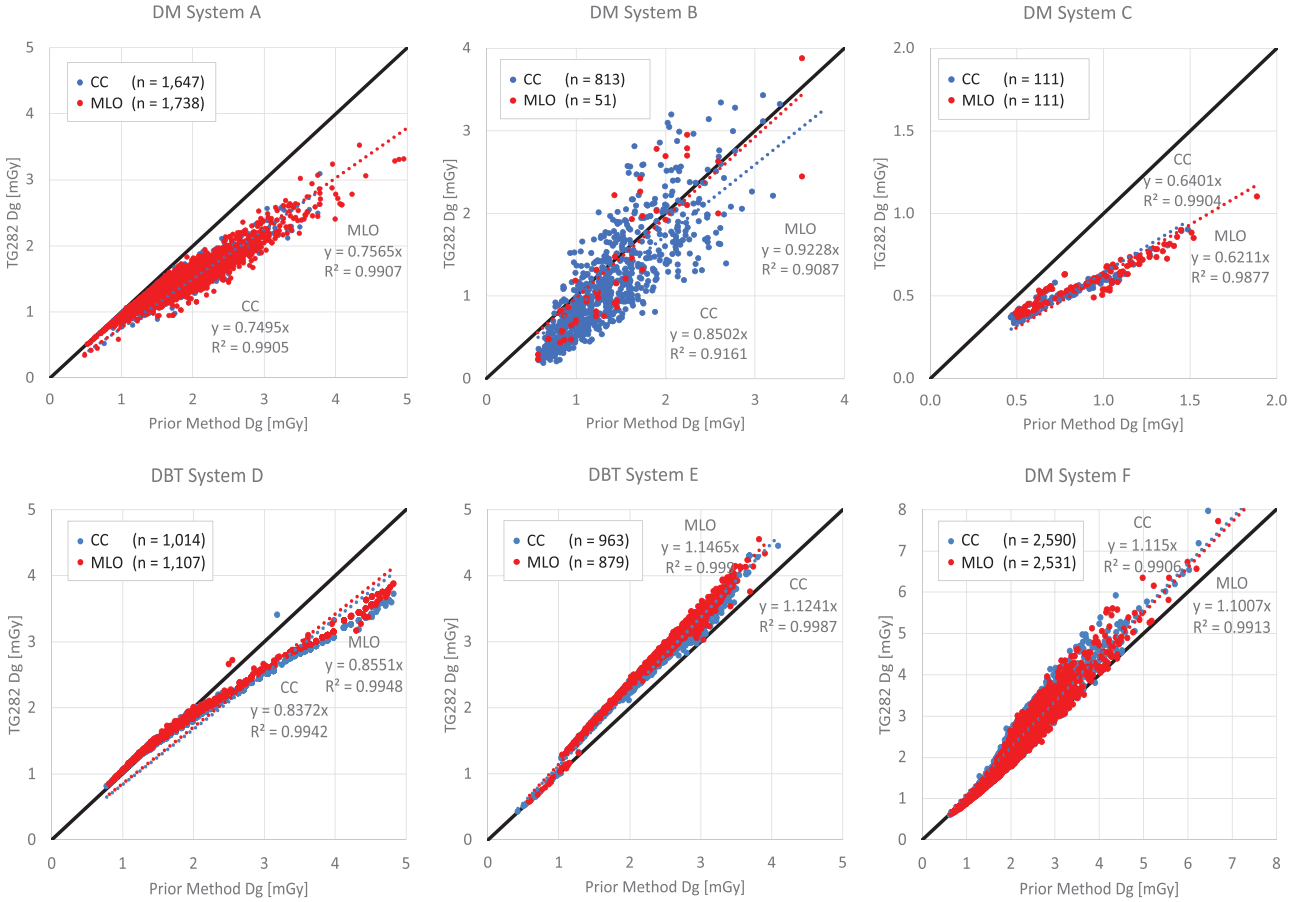

FIGURE C.1 Comparison of average glandular dose estimates for 13 555 digital mammography and digital breast tomosynthesis acquisitions of diagnostic and screening exams, for five different vendor systems, from five different sites. Please note the different ranges of values used in each graph.

breast thickness and view, as done automatically by the software). Data for both DM and DBT acquisitions from systems from different manufacturers, including both CC and MLO views and the expected wide range of compressed breast thicknesses, was included.

As can be seen in Figure C.1 the average breast glandular dose estimated with the new methodology sometimes results in considerably lower estimates, spanning in reduction from ~15% to ~40%, while for some cases the difference is small or even results in an increase in the D_g estimates, depending on the system being compared. Of course, this ratio varies depending on each case, as can be expected due to intra-acquisition variabilities. It should be noted that the existing D_g estimates for Systems A and B are those output by the imaging system in the DICOM header corresponding to each acquisition, while the estimates for Systems C-F were calculated separately with the Dance method[3,7,8] using the acquisition information obtained from the DICOM header. When sub-analyzing these results, as can be seen in Figure C.1, no substantial differences in these trends were found for the CC vs. the MLO views.

APPENDIX D: DIFFERENCES BETWEEN DOSE ESTIMATES WITH THIS MODEL VS. PATIENT-SPECIFIC DOSE ESTIMATES

A Monte Carlo study was performed to compare the resulting dose estimates when using the new breast

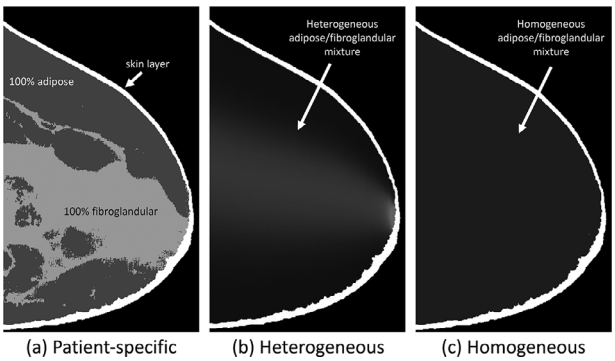

FIGURE D.1 Central slice of one example breast used for the validation of the heterogeneous fibroglandular tissue model. (a) Patient-specific, (b) heterogeneous, and (c) homogeneous fibroglandular tissue distribution model. All three examples contain the same overall glandular fraction (17%). Adapted from Caballo et al, Medical Physics, 2022;49(8): 5423–5438.

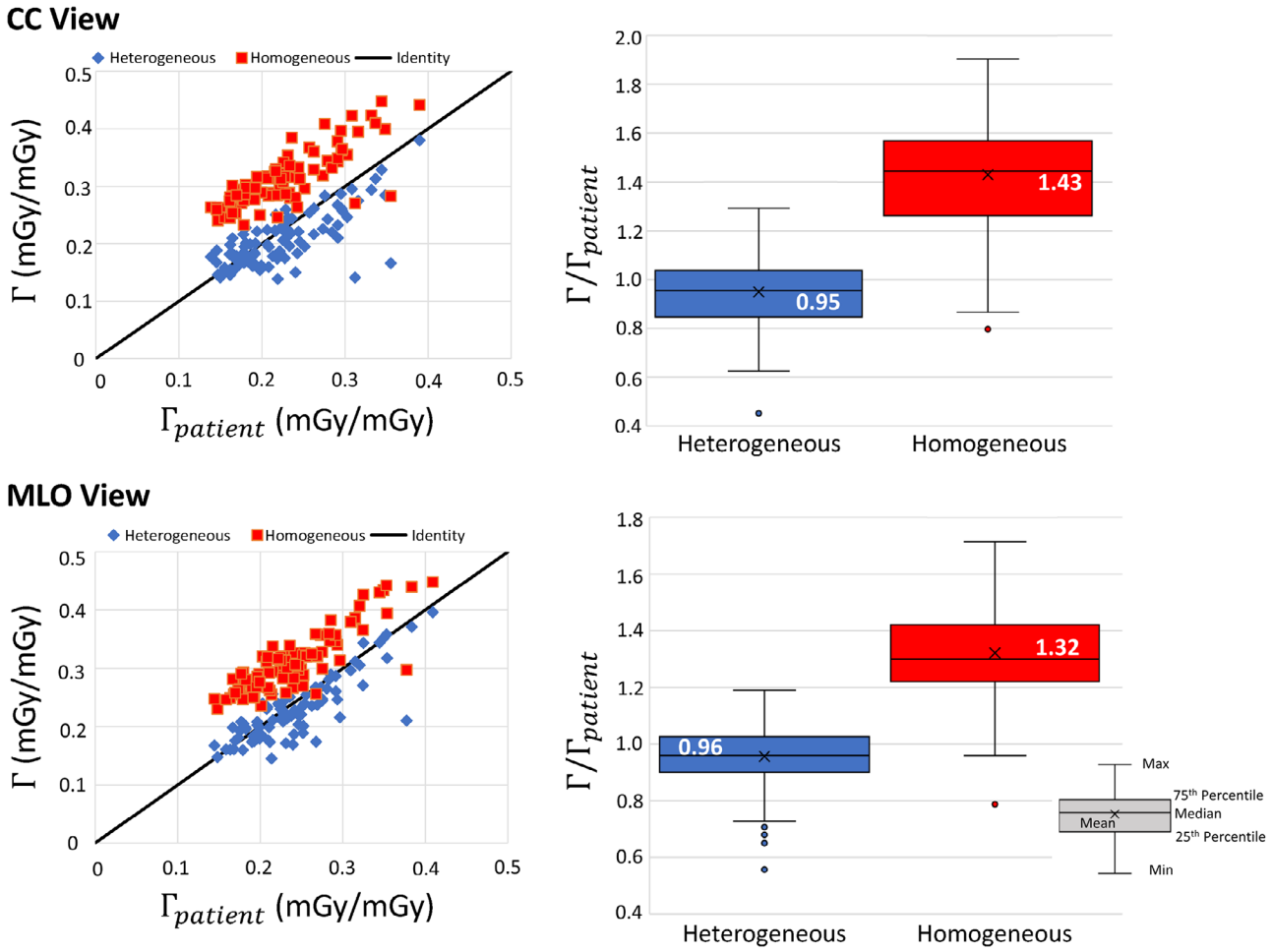

FIGURE D.2 (right) Estimated dose conversion coefficient for the homogeneous and heterogeneous breast models compared to the corresponding patient-based models ones, for the (top) CC and (bottom) MLO views. (left) Box-whisker plots of the ratios of the dose conversion coefficients comparing these same two models to the patient-specific one. The boxes depict the 25th, 50th, and 75th percentiles, the lower and upper whiskers depict the 1.5*interquartile ranges below and above the 25th and 75th percentiles, respectively, and the cross and the specified value are the means. Adapted from Caballo et al, Medical Physics, 2022;49(8): 5423–5438.

model distribution with non-uniform fibroglandular tissue to the original structured distribution found in actual patients' breasts vs. to a uniform homogeneous fibroglandular tissue distribution.[21] In this comparison, only the internal fibroglandular tissue distribution of the three breast representations was modified, while maintaining the breast shape and skin thickness across representations, based on the patient-specific model, as shown in Figure D.1.

As can be seen in Figure D.2, the comparison between the glandular dose estimates resulting from the new non-uniform fibroglandular distribution model and those from the actual patients' fibroglandular distribution show a median deviation of only 5%, while the dose estimates using a homogeneous model show a ~30–45% deviation. Therefore, the new breast fibroglandular distribution model results in a non-biased estimate of the average patient dose. Of course, as explained in Section I, this model dosimetry still reflects large deviations from individual dose estimates of specific patient breasts, which are shown in the box-whisker plots in Figure D.2 as a large variation in the ratio between the dose conversion coefficients for the heterogeneous models versus the patient-specific one. However, individual, patient-specific dose estimates are only achievable with patient-specific dosimetry, which is not the aim of this breast dosimetry model.

It should be noted that this comparison is different from that made in Appendix C, and therefore, as expected, the results of these comparisons differ. The analysis described in this section aims to determine the validity of the heterogeneous fibroglandular tissue distribution, whereas that in Appendix C compares prior dosimetry models to the one proposed here.